AIMS Mathematics, 10(5): 12254–12285.
DOI: 10.3934/math.2025555
Received: 25 February 2025
Revised: 23 April 2025
Accepted: 30 April 2025
Published: 27 May 2025

https://www.aimspress.com/journal/Math

Research article

Exploring families of soliton solutions for the fractional Akbota equation in optical fiber telecommunication systems

Musarat Bibi[1], **Salah Mahmoud Boulaaras**[2], **Patricia J.Y. Wong**[3,*] **and Muhammad Shoaib Saleem**[1,4]

[1] Department of Mathematics, University of Okara, Okara, Pakistan
[2] Department of Mathematics, College of Science, Qassim University, Buraydah, Saudi Arabia
[3] School of Electrical and Electronic Engineering, Nanyang Technological University, Singapore
[4] Center of Theoretical Physics, Khazar University, Baku, Azerbaijan

* **Correspondence:** Email: ejywong@ntu.edu.sg.

Abstract: This work examined new analytical soliton solutions of the conformable fractional nonlinear (1+1)-dimensional Akbota problem utilizing the modified extended direct algebraic technique and a new Kudryashov method. This study investigated the application of the fractional Akbota equation in optical fiber telecommunications, where soliton solutions are crucial for maintaining signal integrity over long distances. Akbota is an integrable equation of the Heisenberg ferromagnetic variety, and it holds considerable importance for surface geometry and curve analysis in optics and magnetism. The derived soliton solutions might be characterized as dark, bright, periodic, or in other forms. The results collected are validated and shown in three-dimensional and two-dimensional graphs. The utilization of fractional derivatives has yielded results that are more contemporary than those presently found in the literature. The findings indicate that the fractional variant of the Akbota equation enhances modeling precision for nonlinear phenomena in optical fibers, rendering it an essential instrument for improving fiber optic networks. Consequently, the derived answers are beneficial for subsequent investigations of this model. The utilized methodologies yield a variety of solutions. In conclusion, the applied techniques are straightforward, effective, and dependable for solving other different models in mathematical physics. The novelty of this work lies in the application of the conformable fractional approach to the Akbota equation system, along with the implementation of new analytical methods that reveal a broader spectrum of soliton solutions, including bright, dark, periodic-singular, and breather structures, many of which have not been previously reported for this model.

Keywords: modified extended direct algebraic method; new Kudryashov method; fractional Akobta equation; solitons; nonlinear equations
Mathematics Subject Classification: 35C08

1. Introduction

In physics and other scientific fields such as differential geometry of curves and surfaces, fractional partial differential equations are essential. Nonlinear fractional partial differential equations (NFPDEs) represent several realistic models of phenomena in various sectors of applications like mathematical physics [1], science and engineering [2], biology [3], financial modeling [4], and fluid dynamics [5,6]. Investigating these NFPDEs is an extremely challenging task. That being said, there exist a subset of NFPDEs known as the integrable equations. Different methods can be used to solve these integrable NFPDEs and produce precise analytical answers for soliton problems. These include the extended sinh-Gordon equation expansion technique [7,8], the generalized exponential rational function technique [9,10], the unified technique [11], the (G'/G^2)-expansion technique [12,13], the homotopy perturbation transform method [14], bifurcation analysis [15], the explicit finite difference method [16], the local fractional homotopy method [17], and many more [18–20]. It was discovered that the so-called gauge equivalences provide a relationship between some integrable equations. A system that can be integrated is the Akbota equation (AE), represented as follows [21–23]:

$$\begin{aligned} \iota\phi_t + \alpha\phi_{xx} + \beta\phi_{xt} + \gamma\psi\phi = 0, \\ \psi_x + 2\epsilon(\alpha|\phi|_x^2 + \beta|\phi|_t^2) = 0, \end{aligned} \tag{1.1}$$

where $\psi = \psi(x,t)$ is a real function, $\phi = \phi(x,t)$ is a complex function, and $\epsilon = 1$. Arbitrary constants α, β, and γ are also present. The system's equivalent gauge counterpart (1.1) takes the following form:

$$\begin{aligned} \iota D_t^\rho\phi + \alpha D_{xx}^{2\rho}\phi + \beta D_{xt}^{2\rho}\phi + \gamma\psi\phi = 0, \\ D_x^\rho\psi + 2\epsilon(\alpha D_x^\rho|\phi|^2 + \beta D_t^\rho|\phi|^2) = 0, \end{aligned} \tag{1.2}$$

where D_x^ρ denotes the conformable fractional derivative. The conformable fractional derivative is introduced to capture memory and nonlocal effects in the Akbota model [24,25], offering a more realistic framework for describing nonlinear wave propagation in optical fiber systems. Equation (1.2) is a fractional generalization of the traditional Akbota system (1.1) and is proposed in order to include the effects of memory and nonlocal interactions through the use of the conformable fractional derivative. The fact that the model includes the fractional derivative allows it to provide more sophisticated dynamical behaviors that often occur in real systems and cannot be addressed well by integer-order models.

We see that introducing the parameter α might look artificial on the surface; however, it plays an essential role in making the system more adaptive and closer to physical processes. In particular, the adaptable parameter α enables the model to control the extent of memory effects, which are very significant within the framework of complex systems like telecommunications and hydrodynamics. When $\alpha = 0$, Eq (1.2) becomes the Kuralay equation, a standard model in its own right. In addition, letting $\beta = 0$ retrieves the familiar nonlinear Schrödinger equation, commonly used to investigate soliton dynamics and wave propagation.

The versatility of Eq (1.2) is that it can interpolate smoothly between various physical models based on the values of α and β, thus it is a versatile tool for modeling a variety of phenomena. Its use of fractional derivatives provides a more powerful framework for investigating complex, memory-dependent systems, yielding insights that are especially useful for applications in fields like

telecommunications, nonlinear optics, and fluid dynamics. The study of the nonlinear phenomena in magnets benefits greatly from the use of the Akbota equation, a Heisenberg ferromagnet-type equation. Analytical solutions are important methodologies in both science research and engineering practice. In addition to developing our understanding of the natural world, analytical solutions also serve to provide a fundamental theoretical basis, which can result in correct control and prediction for systems. With the fact that the Akbota equation appears in a plethora of various areas of science, analytical solutions play a necessary part in understanding the model in all aspects, since analytical solutions permit us to fully comprehend the underlying behavior of the system that the equations model. Their concise and unambiguous nature of representation of the interactions between the variables and the parameters facilitates a better comprehension of the underlying concepts controlling the system.

Researchers focused on the Akbota equation recently (2024) and attempted to talk about a few important facets of the governing model [26,27]. Using Jacobi elliptic functions, the produced dark and brilliant solutions were able to display stability and first-order conserved vectors. There were still, however, a number of important and widespread forms of solitons lacking in the literature. Therefore, this study used the generalized analytical methodologies [28–30] to carry out and establish various kinds of solitons in order to fill this gap. These analytical methods produce multiple diverse families of solutions and are dependent on various differential equations.

This article uses the modified extended direct algebraic method (mEDAM) and new Kudryashov method to investigate solutions of soliton waves of the under examined model. Notably, there is not a single investigation like this one in the body of current literature. Applying this technique produces a wide range of solutions, including trigonometric, hyperbolic, singular, bright, singular periodic, and dark solutions. Several models have been solved in the literature to show how effective this method is.

This study aims to elucidate the impact of the conformable fractional derivative on the space-time fractional Akbota equation solutions obtained through the use of the mEDAM and new Kudryashov method. The fact that the conformable fractional derivative satisfies the requirements of both fractional order and integer derivatives gives it significance. In this research, we have used the conformable fractional form of the Akbota equation system, which is a more realistic model for real systems with memory effects and nonlocal behaviors, like those in telecommunications. The conformable fractional derivative, a new generalization of the classical derivative, has several benefits over conventional integer-order derivatives. Unlike the usual fractional derivative, which brings about considerable complication in computation and interpretation, the conformable fractional derivative preserves more intuitive features without sacrificing the main features of fractional dynamics. It is thus particularly useful for modeling processes such as signal dispersion and attenuation in telecommunications, where wave behavior over large distances entails long-range interactions not captured by integer-order derivatives. Using the conformable fractional derivative, we can then better model these nonlocal effects and thus gain a better understanding of wave propagation and communication system dynamics. Using this method gives a closer representation of physical systems as they exist in the real world, with the possibility of improving the efficiency and reliability of telecommunication networks.

We can see some basic relationships between fractional nonlinear partial differential equations (FNPDEs) and other simple nonlinear partial differential equations by using our scheme. It has been discovered that several types of precise wave solutions of some complex FNPDEs can be readily produced with the aid of straightforward schemes and solvable ordinary differential equations. Partial differential equations with nonlinearities are solved using this method. To identify the several

categories of precise wave solutions, this approach is suggested. We obtain solutions that are extremely near to the numerical solutions by employing the conformable fractional derivative. Since the conformable fractional derivative and the employed technique are novel for the model in question, our obtained solutions outperform the current ones. 2D graphs also illustrate the influence of conformable fractional derivatives.

While several studies have investigated soliton solutions in nonlinear classical systems, there has been limited research focusing on the fractional form of the Akbota equation with conformable derivatives. Additionally, the majority of works that exist have not conducted an extensive study on different soliton behaviors, such as periodic-singular and breather-type configurations. To fill this gap, our research presents a fractional generalization of the Akbota system and applies both traditional and newly developed analytical techniques to obtain a rich variety of exact solutions. A thorough comparison between various orders of fractions has been made to demonstrate how the fractional parameter affects the shape, amplitude, and propagation behavior of the soliton solutions. In addition, the stability of some solutions has been examined to ensure their physical significance. The innovation of our methodology is not just in the conformable fractional modeling but also in the variety and physical meaning of the resulting soliton structures such as bright, dark, periodic-singular, and breather solitons, which provide new information about nonlinear wave propagation and possible applications in telecommunication systems and nonlinear optical media.

The structure of this article is as follows. The next section describes the conformable fractional derivative. Section 3 offers a synopsis of the suggested integration techniques. Section 4 presents the retrieved solutions of the proposed models. Section 5 presents the results and discussion. Ultimately, Section 6 brings the work to a close.

2. Conformable fractional derivative and its properties

The conformable fractional derivative is a novel, interesting definition of the fractional derivative that was just developed by writers Khalil et al. [31]. The Leibniz rule and chain rule are both followed by this derivative, which is well-behaved. Here, we define the conformable fractional derivative and list a few helpful characteristics of this brand-new derivative [32].

Definition 2.1. Given a function $f : (0, \infty) \to R$, the conformable fractional derivative of f with order α, $0 < \alpha \leq 1$, can be calculated as

$$D^{\alpha} f(t) = \lim_{\varepsilon \to 0} \frac{f(t + \varepsilon t^{1-\alpha}) - f(t)}{\varepsilon}, \quad \forall\, t > 0.$$

Here is a list of some beneficial attributes:

Properties 2.1.

- Linearity: $D^{\alpha}(af + bg) = a(D^{\alpha} f) + b(D^{\alpha} g)$, $\forall\, a, b \in R$.
- Leibniz rule: $D^{\alpha}(f.g) = fD^{\alpha} g + gD^{\alpha} f$.
- Chain rule: Let $f : (0, \infty) \to R$ be differentiable and α-differentiable, and g be a differentiable function defined in the range of f.

$$D^{\alpha}(f \circ g)(t) = t^{1-\alpha} g'(t) f'(g(t)).$$

Furthermore, the ensuing guidelines apply.

- $D^{\alpha}(t^{p}) = pt^{p-\alpha}, \ for \ all \ p \in R.$
- $D^{\alpha}(\frac{f}{g}) = \frac{gD^{\alpha}f - fD^{\alpha}g}{g^{2}}$.
- $D^{\alpha}(c) = 0$, where $f(t) = c$ is a constant.
- If f is differentiable, then

$$D^{\alpha}f(t) = t^{1-\alpha}\frac{df}{dt}. \tag{2.1}$$

3. Methodologies

3.1. Modified extended direct algebraic method

The modified EDAM approach is described in this section. Examine the fractional partial differential equation represented by [33–36]

$$E(u, \partial_{t}^{\alpha}u, \partial_{\theta_1}^{\beta}u, \partial_{\theta_2}^{\gamma}u, ...) = 0, \quad 0 < \alpha, \beta, \gamma \leq 1, \tag{3.1}$$

where u is a function of $\theta_1, \theta_2, ..., \theta_r$ and t.

The following are the steps needed to solve Eq (3.1):

Step 1. The variables $u(\theta_1, \theta_2, \theta_3, ..., \theta_r)$ are first transformed into $U(\xi)$, where ξ might be given in a number of ways. This transformation converts Eq (3.1) into a nonlinear ODE of the following form:

$$G(U, U^{'}, U^{''}, ...) = 0, \tag{3.2}$$

when there are derivatives of U with regard to ξ in Eq (3.2). The constant(s) of integration can be obtained by integrating Eq (3.2) one or more times.

Step 2. Next, we will assume that the solution to Eq (3.2) is as follows:

$$U(\xi) = \sum_{j=-\Theta}^{\Theta} f_{j}H^{j}(\xi), \tag{3.3}$$

where f_j ($j = -\Theta, ..., 0, 1, 2, ..., \Theta$) are constants and $H(\xi)$ satisfies the ODE of the form

$$H^{'}(\xi) = Ln(C)(\varkappa + \mu H(\xi) + \beta H^{2}(\xi)). \tag{3.4}$$

It should be noted that while $\varkappa$, μ, and β stay constant throughout the study, C assumes a value other than 0 and 1.

Step 3. The positive integer Θ supplied in Eq (3.3) is obtained by establishing the homogeneous balance between the highest nonlinear term and the highest-order derivative in Eq (3.2). More specifically, the two provided formulas [37] can be used to estimate the balance number:

$$D(\frac{d^{k}U}{d\xi^{k}}) = \Theta + k, \text{ and } D(U^{l}(\frac{d^{k}U}{d\xi^{k}})^{j}) = \Theta l + j(k + \Theta),$$

where D stands for the degree of $U(\xi)$ as $D[U(\xi)] = \Theta$ and j, k, and l are positive integers.

Step 4. Next, we substitute Eq (3.3) into Eq (3.2) or the resulting equation from integrating Eq (3.2), and we set the $h(\xi)$ terms in the same order. After setting all of the coefficients of the next polynomial

to zero, an algebraic system of equations for f_j ($j = -\Theta, ..., 0, 1, 2, ..., \Theta$) and extra parameters are produced.

Step 5. We utilize Mathematica to solve this set of algebraic equations.

Step 6. Next, by figuring out the unknown values and adding them to Eq (3.3) along with $H(\xi)$ (Eq (3.4) solution), the analytical answers to Eq (3.3) are found. The following families of solutions can be generated by applying the general solution of Eq (3.4).

(1) If $\mu^2 - 4\varkappa\beta < 0$ and $\beta \neq 0$, then

$$\begin{aligned}
H_1(\xi) &= -\frac{\mu}{2\beta} + \frac{\sqrt{-(\mu^2-4\varkappa\beta)}}{2\beta} tan_C(\frac{\sqrt{-(\mu^2-4\varkappa\beta)}}{2}\xi),\\
H_2(\xi) &= -\frac{\mu}{2\beta} - \frac{\sqrt{-(\mu^2-4\varkappa\beta)}}{2\beta} cot_C(\frac{\sqrt{-(\mu^2-4\varkappa\beta)}}{2}\xi),\\
H_3(\xi) &= -\frac{\mu}{2\beta} + \frac{\sqrt{-(\mu^2-4\varkappa\beta)}}{2\beta} (tan_C(\sqrt{-(\mu^2-4\varkappa\beta)}\xi) \pm \sqrt{pq} sec_C(\sqrt{-(\mu^2-4\varkappa\beta)}\xi)),\\
H_4(\xi) &= -\frac{\mu}{2\beta} - \frac{\sqrt{-(\mu^2-4\varkappa\beta)}}{2\beta} (cot_C(\sqrt{-(\mu^2-4\varkappa\beta)}\xi) \pm \sqrt{pq} csc_C(\sqrt{-(\mu^2-4\varkappa\beta)}\xi)),\\
H_5(\xi) &= -\frac{\mu}{2\beta} + \frac{\sqrt{-(\mu^2-4\varkappa\beta)}}{4\beta} (tan_C(\frac{\sqrt{-(\mu^2-4\varkappa\beta)}}{4}\xi) - cot_C\frac{(\sqrt{-(\mu^2-4\varkappa)\beta})}{4}\xi)).
\end{aligned}$$

(2) If $\mu^2 - 4\varkappa\beta > 0$ and $\beta \neq 0$, then

$$\begin{aligned}
H_6(\xi) &= -\frac{\mu}{2\beta} - \frac{\sqrt{(\mu^2-4\varkappa\beta)}}{2\beta} tanh_C(\frac{\sqrt{(\mu^2-4\varkappa\beta)}}{2}\xi),\\
H_7(\xi) &= -\frac{\mu}{2\beta} - \frac{\sqrt{(\mu^2-4\varkappa\beta)}}{2\beta} coth_C(\frac{\sqrt{(\mu^2-4\varkappa\beta)}}{2}\xi),\\
H_8(\xi) &= -\frac{\mu}{2\beta} - \frac{\sqrt{\mu^2-4\varkappa\beta}}{2\beta} (tanh_C(\sqrt{\mu^2-4\varkappa\beta}\xi) \pm \iota\sqrt{pq} sech_C(\sqrt{\mu^2-4\varkappa\beta})),\\
H_9(\xi) &= -\frac{\mu}{2\beta} - \frac{\sqrt{(\mu^2-4\varkappa\beta)}}{2\beta} (coth_C(\sqrt{(\mu^2-4\varkappa\beta)}\xi) \pm \sqrt{pq} csch_C(\sqrt{(\mu^2-4\varkappa\beta)}\xi)),\\
H_{10}(\xi) &= -\frac{\mu}{2\beta} - \frac{\sqrt{(\mu^2-4\varkappa\beta)}}{4\beta} (tanh_C(\frac{\sqrt{(\mu^2-4\varkappa\beta)}}{4}\xi) + coth_C(\frac{(\sqrt{(\mu^2-4\varkappa\beta)})}{4}\xi)).
\end{aligned}$$

(3) If $\varkappa\beta > 0$ and $\mu = 0$, then

$$\begin{aligned}
H_{11}(\xi) &= \sqrt{\frac{\varkappa}{\beta}} tan_C(\sqrt{\varkappa\beta}\xi),\\
H_{12}(\xi) &= -\sqrt{\frac{\varkappa}{\beta}} cot_C(\sqrt{\varkappa\beta}\xi),\\
H_{13}(\xi) &= \sqrt{\frac{\varkappa}{\beta}} (tan_C(2\sqrt{\varkappa\beta}\xi) \pm \sqrt{pq} sec_C(2\sqrt{\varkappa\beta}\xi)),\\
H_{14}(\xi) &= -\sqrt{\frac{\varkappa}{\beta}} (cot_C(2\sqrt{\varkappa\beta}\xi) \pm \sqrt{pq} csc_C(2\sqrt{\varkappa\beta}\xi)),
\end{aligned}$$

$$H_{15}(\xi) = \frac{1}{2}\sqrt{\frac{\varkappa}{\beta}}(tan_C(\frac{\sqrt{\varkappa\beta}}{2}\xi) - cot_C(\frac{\sqrt{\varkappa\beta}}{2}\xi)).$$

(4) If $\varkappa\beta < 0$ and $\mu = 0$, then

$$\begin{aligned}
H_{16}(\xi) &= -\sqrt{-\frac{\varkappa}{\beta}}tanh_C(\sqrt{-\varkappa\beta}\xi),\\
H_{17}(\xi) &= -\sqrt{-\frac{\varkappa}{\beta}}coth_C(\sqrt{-\varkappa\beta}\xi),\\
H_{18}(\xi) &= -\sqrt{-\frac{\varkappa}{\beta}}(tanh_C(2\sqrt{-\varkappa\beta}\xi) \pm \iota\sqrt{pq}sech_C(2\sqrt{-\varkappa\beta}\xi)),\\
H_{19}(\xi) &= -\sqrt{-\frac{\varkappa}{\beta}}(coth_C(2\sqrt{-\varkappa\beta}\xi) \pm \sqrt{pq}csch_C(2\sqrt{-\varkappa\beta}\xi)),\\
H_{20}(\xi) &= -\frac{1}{2}\sqrt{-\frac{\varkappa}{\beta}}(tanh_C(\frac{\sqrt{-\varkappa\beta}}{2}\xi) + coth_C(\frac{\sqrt{-\varkappa\beta}}{2}\xi)).
\end{aligned}$$

(5) If $\mu = 0$ and $\beta = \varkappa$, then

$$\begin{aligned}
H_{21}(\xi) &= tan_C(\varkappa\xi),\\
H_{22}(\xi) &= -cot_C(\varkappa\xi),\\
H_{23}(\xi) &= tan_C(2\varkappa\xi) \pm \sqrt{pq}sec_C(2\varkappa\xi),\\
H_{24}(\xi) &= -cot_C(2\varkappa\xi) \pm \sqrt{pq}csc_C(2\varkappa\xi),\\
H_{25}(\xi) &= \frac{1}{2}(tan_C(\frac{\varkappa}{2}\xi) - cot_C(\frac{\varkappa}{2}\xi)).
\end{aligned}$$

(6) If $\mu = 0$ and $\beta = -\varkappa$, then

$$\begin{aligned}
H_{26}(\xi) &= -tanh_C(\varkappa\xi),\\
H_{27}(\xi) &= -coth_C(\varkappa\xi),\\
H_{28}(\xi) &= -tanh_C(2\varkappa\xi) \pm \iota\sqrt{pq}sech_C(2\varkappa\xi),\\
H_{29}(\xi) &= -coth_C(2\varkappa\xi) \pm \sqrt{pq}csch_C(2\varkappa\xi),\\
H_{30}(\xi) &= -\frac{1}{2}(tanh_C(\frac{\varkappa}{2}\xi) + coth_C(\frac{\varkappa}{2}\xi)).
\end{aligned}$$

(7) If $\mu^2 = 4\varkappa\beta$, then

$$H_{31}(\xi) = \frac{-2\varkappa(\mu\xi LnC + 2)}{\mu^2\xi LnC}.$$

(8) If $\mu = \lambda$, $\varkappa = m\lambda$ $(m \neq 0)$, and $\beta = 0$, then

$$H_{32}(\xi) = C^{\lambda\xi} - m.$$

(9) If $\mu = \beta = 0$, then

$$H_{33}(\xi) = \varkappa\xi LnC.$$

(10) If $\mu = \varkappa = 0$, then

$$H_{34}(\xi) = \frac{-1}{\beta\xi LnC}.$$

(11) If $\varkappa = 0$ and $\mu \neq 0$, then

$$H_{35}(\xi) = -\frac{p\mu}{\beta(cosh_C(\mu\xi) - sinh_C(\mu\xi) + p)},$$
$$H_{36}(\xi) = -\frac{\mu(sinh_C(\mu\xi) + cosh_C(\mu\xi))}{\beta(sinh_C(\mu\xi) + cosh_C(\mu\xi) + q)}.$$

(12) If $\mu = \lambda, \beta = m\lambda$ $(m \neq 0)$, and $\varkappa = 0$, then

$$H_{37}(\xi) = \frac{pC^{\lambda\xi}}{q - mpC^{\lambda\xi}}.$$

In the above cases (1)–(12), $p, q > 0$ are defined as deformation parameters. The generalized hyperbolic and triangular functions are defined as follows:

$$sinh_C(\xi) = \frac{pC^{\xi} - qC^{-\xi}}{2}, \quad cosh_C(\xi) = \frac{pC^{\xi} + qC^{-\xi}}{2},$$

$$tanh_C(\xi) = \frac{pC^{\xi} - qC^{-\xi}}{pC^{\xi} + qC^{-\xi}}, \quad coth_C(\xi) = \frac{pC^{\xi} + qC^{-\xi}}{pC^{\xi} - qC^{-\xi}},$$

$$sech_C(\xi) = \frac{2}{pC^{\xi} + qC^{-\xi}}, \quad csch_C(\xi) = \frac{2}{pC^{\xi} - qC^{-\xi}},$$

$$sin_C(\xi) = \frac{pC^{\iota\xi} - qC^{-\iota\xi}}{2\iota}, \quad cos_C(\xi) = \frac{pC^{\iota\xi} + qC^{-\iota\xi}}{2},$$

$$tan_C(\xi) = -\iota\frac{pC^{\iota\xi} - qC^{-\iota\xi}}{pC^{\iota\xi} + qC^{-\iota\xi}}, \quad cot_C(\xi) = \iota\frac{pC^{\iota\xi} + qC^{-\iota\xi}}{pC^{\iota\xi} - qC^{-\iota\xi}},$$

$$sec_C(\xi) = \frac{2}{pC^{\iota\xi} + qC^{-\iota\xi}}, \quad csc_C(\xi) = \frac{2\iota}{pC^{\iota\xi} - qC^{-\iota\xi}}.$$

3.2. New Kudryashov method

Typically, Kudryashov approaches utilize the logistic function to examine the analytical solutions of NPDEs [38–40]. However, the Kudryashov approaches, which depend on the logistic function, prove inadequate in producing optical soliton solutions due to the distinctive structure of nonlinear partial differential equations (NPDEs) introduced by the extended Schrödinger equations. Therefore, in this investigation, we propose a novel technique based on the Kudryashov approach. This method

employs a distinct function intentionally designed to effectively handle the intricacies and prerequisites associated with deriving optical soliton solutions. The novel approach relies on this function [41]:

$$H(\xi) = \frac{2\nu B}{B^2 e^{\nu\sigma\xi} \mp m e^{\nu\sigma\xi}}, \tag{3.5}$$

and the hyperbolic form is

$$H(\xi) = \frac{2\nu B}{(B^2 \mp m)cosh(\sigma\xi) + (B^2 \pm m)sinh(\sigma\xi)}, \tag{3.6}$$

where $\nu = \mp 1, B, m$ are constants, and $H(\xi)$ satisfies the following equation:

$$(\frac{dH(\xi)}{d\xi})^2 - \sigma^2 H^2(\xi)(1 \pm mH^2(\xi)) = 0. \tag{3.7}$$

The solutions provided by the current approach represent the following series solution for the analyzed model:

$$U(\xi) = \sum_{j=0}^{\Theta} f_j H^j(\xi), \quad f_\Theta \neq 0. \tag{3.8}$$

The values $f_0, f_1, \ldots$ are the unknowns and Θ is the balancing value.

4. Mathematical analysis of the controlling model

Take into account the traveling wave transformations:

$$\phi(x,t) = U(\eta)e^{\iota(-kx+\omega t)}, \ \ \psi(x,t) = V(\eta), \tag{4.1}$$

where $\eta = \frac{x^\rho}{\rho} - k_2\frac{t^\rho}{\rho}$, replacing transformation Eq (4.1) with Eq (1.2) and dividing the real and imaginary parts:

$$(\alpha - k_2\delta)U'' + (-\omega - \alpha k^2 + \delta k\omega + \gamma V)U = 0, \tag{4.2}$$

$$(-k_2 - 2\alpha k + \delta k k_2 + \delta\omega)U' = 0, \tag{4.3}$$

$$V' - 2\epsilon(2\alpha UU' - 2\delta k_2 UU') = 0. \tag{4.4}$$

From Eq (4.3), we get

$$\omega = \frac{k_2 + 2\alpha k - \delta k k_2}{\delta}. \tag{4.5}$$

Integrating Eq (4.4), we obtain

$$V = 2\epsilon(\alpha - \delta k_2)U^2. \tag{4.6}$$

Equations (4.5) and (4.6) are substituted into Eq (4.2), yielding the following ODE:

$$\delta(\alpha - k_2\delta)U'' + (-k_2 + k(-2 + \delta k)(\alpha - k_2\delta))U + 2\delta\gamma\epsilon(\alpha - k_2\delta)U^3 = 0, \tag{4.7}$$

where $(\alpha - k_2\delta) \neq 0$. Now, from the balancing condition on Eq (4.7) between the highest-order derivative term U'' with the highest-power nonlinear term U^3, $\Theta + 2 = 3\Theta \implies \Theta = 1$.

4.1. Application of mEDAM

Put $\Theta = 1$ in Eq (3.3) in order to use mEDAM to solve the NODE in Eq (4.8) that is produced from the fractional Akbota equation. Consequently, we have

$$U(\eta) = c_{-1}H^{-1}(\eta) + c_0 + c_1 H(\eta). \tag{4.8}$$

By replacing the expression Eq (4.8) into Eq (4.7) and setting the coefficients of $U(\eta)$ equal to zero, we derive a set of algebraic equations.

$$\begin{aligned}
(H(\eta))^0 \quad &: \quad (\beta\delta\mu Ln[A]^2 c_{-1}(\alpha - \delta k_2) + 2\gamma\delta\epsilon c_0^3(\alpha - \delta k_2) + \delta\mu\chi Ln[A]^2 c_1(\alpha - \delta k_2) \\
&\quad +12\gamma\delta\epsilon c_{-1}c_0c_1(\alpha - \delta k_2) + c_0(k_2 + k(-2 + k\delta)(\alpha] - \delta]k_2))) = 0, \\
(H(\eta))^{-3} \quad &: \quad (2\delta\chi^2 Ln[A]^2 c_{-1}(\alpha - \delta k_2) + 2\gamma\delta\epsilon c_{-1}^3(\alpha - \delta k_2)) = 0, \\
(H(\eta))^{-2} \quad &: \quad (3\delta\mu\chi Ln[A]^2 c_{-1}(\alpha - \delta]k_2) + 6\gamma\delta\epsilon]c_{-1}^2 c_0(\alpha - \delta k_2)) = 0, \\
(H(\eta))^{-1} \quad &: \quad (\delta\mu]^2 Ln[A]^2 c_{-1}(\alpha - \delta k_2) + 2\beta\delta\chi Ln[A]^2 c_{-1}(\alpha] - \delta k_2) + 6\gamma\delta\epsilon c_{-1}c_0^2(\alpha - \delta k_2) \\
&\quad +6\gamma\delta\epsilon c_{-1}^2 c_1(\alpha - \delta k_2) + c_{-1}(-k_2 + k(-2 + k\delta)(\alpha - \delta k_2))) = 0, \\
(H(\eta))^{1} \quad &: \quad (\delta\mu^2 Ln[A]^2 c_1(\alpha - \delta k_2) + 2\beta\delta\chi Ln[A]^2 c_1(\alpha - \delta k_2) + 6\gamma\delta\epsilon c_0^2 c_1(\alpha - \delta k_2) \\
&\quad +6\gamma\delta\epsilon c_{-1}c_1^2(\alpha - \delta k_2 + c_1(-k_2 + k(-2 + k\delta)(\alpha - \delta k_2))) = 0, \\
(H(\eta))^{2} \quad &: \quad (3\beta\delta\mu Ln[A]^2 c_1(\alpha - \delta k_2) + 6\gamma\delta\epsilon c_0 c_1^2(\alpha - \delta k_2)) = 0, \\
(H(\eta))^{3} \quad &: \quad (2\beta^2\delta Ln[A]^2 c_1(\alpha - \delta k_2) + 2\gamma\delta\epsilon c_1^3(\alpha - \delta k_2)) = 0.
\end{aligned}$$

By solving this system, we obtain two distinct cases of solutions:
Case 1.

$$c_0 = c_0,\ c_1 = \frac{2\beta c_0}{\mu},\ c_{-1} = 0,\ \epsilon = \frac{\mu^2(Ln(C))^2}{4\beta c_0^2},\ \alpha = \frac{(2(1 - 2\delta k(2 - \delta)) - \delta^2 Ln(C)^2 M)k_2}{2k(\delta k - 2) - \delta Ln(C)^2 M}. \tag{4.9}$$

Case 2.

$$c_0 = c_0,\ c_1 = 0,\ c_{-1} = \frac{2\varkappa c_0}{\mu},\ \epsilon = \frac{\mu^2(Ln(C))^2}{4\beta c_0^2},\ \alpha = \frac{(2(1 - 2\delta k(2 - \delta)) - \delta^2 Ln(C)^2 M)k_2}{2k(\delta k - 2) - \delta Ln(C)^2 M}, \tag{4.10}$$

where $M = \mu^2 - 4\varkappa\beta$.

Considering Case 1, the following families of solutions result:
Family 1. When $M < 0$ and $\beta \neq 0$, then

$$U_1(\eta) = c_0 + \frac{2\beta c_0}{\mu}[-\frac{\mu}{2\beta} + \frac{\sqrt{-M}}{2\beta} tan_C(\frac{\sqrt{-M}}{2}\eta)]. \tag{4.11}$$

The following solitary wave solutions for (1.2) are obtained with the help of (4.1) and (4.6):

$$\phi_1(\eta) = (c_0 + \frac{2\beta c_0}{\mu}[-\frac{\mu}{2\beta} + \frac{\sqrt{-M}}{2\beta} tan_C(\frac{\sqrt{-M}}{2}\eta)])e^{\iota(-kx+\omega t)}, \tag{4.12}$$

and

$$\psi_1(\eta) = 2\epsilon(\alpha - \delta k_2)(c_0 + \frac{2\beta c_0}{\mu}[-\frac{\mu}{2\beta} + \frac{\sqrt{-M}}{2\beta} tan_C(\frac{\sqrt{-M}}{2}\eta)])^2, \tag{4.13}$$

$$U_2(\eta) = c_0 + \frac{2\beta c_0}{\mu}[-\frac{\mu}{2\beta} + \frac{\sqrt{-M}}{2\beta}cot_C(\frac{\sqrt{-M}}{2}\eta)]. \tag{4.14}$$

The following solitary wave solutions for (1.2) are obtained with the aid of (4.1) and (4.6):

$$\phi_2(\eta) = (c_0 + \frac{2\beta c_0}{\mu}[-\frac{\mu}{2\beta} + \frac{\sqrt{-M}}{2\beta}cot_C(\frac{\sqrt{-M}}{2}\eta)])e^{\iota(-kx+\omega t)}, \tag{4.15}$$

and

$$\psi_2(\eta) = 2\epsilon(\alpha - \delta k_2)(c_0 + \frac{2\beta c_0}{\mu}[-\frac{\mu}{2\beta} + \frac{\sqrt{-M}}{2\beta}cot_C(\frac{\sqrt{-M}}{2}\eta)])^2, \tag{4.16}$$

$$U_3(\eta) = c_0 + \frac{2\beta c_0}{\mu}[-\frac{\mu}{2\beta} + \frac{\sqrt{-M}}{2\beta}(tan_C(\sqrt{-M}\eta) \pm \sqrt{pq}sec_C(\sqrt{-M}\eta))]. \tag{4.17}$$

The following solitary wave solutions for (1.2) are obtained with the help of (4.1) and (4.6):

$$\phi_3(\eta) = (c_0 + \frac{2\beta c_0}{\mu}[-\frac{\mu}{2\beta} + \frac{\sqrt{-M}}{2\beta}(tan_C(\sqrt{-M}\eta) \pm \sqrt{pq}sec_C(\sqrt{-M}\eta))])e^{\iota(-kx+\omega t)}, \tag{4.18}$$

and

$$\psi_3(\eta) = 2\epsilon(\alpha - \delta k_2)(c_0 + \frac{2\beta c_0}{\mu}[-\frac{\mu}{2\beta} + \frac{\sqrt{-M}}{2\beta}(tan_C(\sqrt{-M}\eta) \pm \sqrt{pq}sec_C(\sqrt{-M}\eta))])^2, \tag{4.19}$$

$$U_4(\eta) = c_0 + \frac{2\beta c_0}{\mu}[-\frac{\mu}{2\beta} + \frac{\sqrt{-M}}{2\beta}(cot_C(\sqrt{-M}\eta) \pm \sqrt{pq}csc_C(\sqrt{-M}\eta))]. \tag{4.20}$$

The following solitary wave solutions for (1.2) are obtained with the aid of (4.1) and (4.6):

$$\phi_4(\eta) = (c_0 + \frac{2\beta c_0}{\mu}[-\frac{\mu}{2\beta} + \frac{\sqrt{-M}}{2\beta}(cot_C(\sqrt{-M}\eta) \pm \sqrt{pq}csc_C(\sqrt{-M}\eta))])e^{\iota(-kx+\omega t)}, \tag{4.21}$$

and

$$\psi_4(\eta) = 2\epsilon(\alpha - \delta k_2)(c_0 + \frac{2\beta c_0}{\mu}[-\frac{\mu}{2\beta} + \frac{\sqrt{-M}}{2\beta}(cot_C(\sqrt{-M}\eta) \pm \sqrt{pq}csc_C(\sqrt{-M}\eta))])^2, \tag{4.22}$$

$$U_5(\eta) = c_0 + \frac{2\beta c_0}{\mu}[-\frac{\mu}{2\beta} + \frac{\sqrt{-M}}{4\beta}(tan_C(\frac{\sqrt{-M}}{4}\eta) - cot_C(\frac{\sqrt{-M}}{4}\eta))]. \tag{4.23}$$

The following solitary wave solutions for (1.2) are obtained with the aid of (4.1) and (4.6):

$$\phi_5(\eta) = (c_0 + \frac{2\beta c_0}{\mu}[-\frac{\mu}{2\beta} + \frac{\sqrt{-M}}{4\beta}(tan_C(\frac{\sqrt{-M}}{4}\eta) - cot_C(\frac{\sqrt{-M}}{4}\eta))])e^{\iota(-kx+\omega t)}, \tag{4.24}$$

and

$$\psi_5(\eta) = 2\epsilon(\alpha - \delta k_2)(c_0 + \frac{2\beta c_0}{\mu}[-\frac{\mu}{2\beta} + \frac{\sqrt{-M}}{4\beta}(tan_C(\frac{\sqrt{-M}}{4}\eta) - cot_C(\frac{\sqrt{-M}}{4}\eta))])^2. \tag{4.25}$$

All the solutions of Family 1 are stable under the condition $M < 0$, ensuring their physical relevance and stability.

Family 2. When $M > 0$ and $\beta \neq 0$, then

$$U_6(\eta) = c_0 + \frac{2\beta c_0}{\mu}[-\frac{\mu}{2\beta} + \frac{\sqrt{M}}{2\beta}tanh_C(\frac{\sqrt{M}}{2}\eta)]. \tag{4.26}$$

The following solitary wave solutions for (1.2) are obtained with the aid of (4.1) and (4.6):

$$\phi_6(\eta) = (c_0 + \frac{2\beta c_0}{\mu}[-\frac{\mu}{2\beta} + \frac{\sqrt{M}}{2\beta}tanh_C(\frac{\sqrt{M}}{2}\eta)])e^{\iota(-kx+\omega t)}, \tag{4.27}$$

and

$$\psi_6(\eta) = 2\epsilon(\alpha - \delta k_2)(c_0 + \frac{2\beta c_0}{\mu}[-\frac{\mu}{2\beta} + \frac{\sqrt{M}}{2\beta}tanh_C(\frac{\sqrt{M}}{2}\eta)])^2, \tag{4.28}$$

$$U_7(\eta) = c_0 + \frac{2\beta c_0}{\mu}[-\frac{\mu}{2\beta} + \frac{\sqrt{M}}{2\beta}coth_C(\frac{\sqrt{M}}{2}\eta)]. \tag{4.29}$$

The following solitary wave solutions for (1.2) are obtained with the aid of (4.1) and (4.6):

$$\phi_7(\eta) = (c_0 + \frac{2\beta c_0}{\mu}[-\frac{\mu}{2\beta} + \frac{\sqrt{M}}{2\beta}coth_C(\frac{\sqrt{M}}{2}\eta)])e^{\iota(-kx+\omega t)}, \tag{4.30}$$

and

$$\psi_7(\eta) = 2\epsilon(\alpha - \delta k_2)(c_0 + \frac{2\beta c_0}{\mu}[-\frac{\mu}{2\beta} + \frac{\sqrt{M}}{2\beta}coth_C(\frac{\sqrt{M}}{2}\eta)])^2, \tag{4.31}$$

$$U_8(\eta) = c_0 + \frac{2\beta c_0}{\mu}[-\frac{\mu}{2\beta} + \frac{\sqrt{M}}{2\beta}(tanh_C(\sqrt{M}\eta) \pm \iota\sqrt{pq}sech_C(\sqrt{M}\eta))]. \tag{4.32}$$

The following solitary wave solutions for (1.2) are obtained with the aid of (4.1) and (4.6):

$$\phi_8(\eta) = (c_0 + \frac{2\beta c_0}{\mu}[-\frac{\mu}{2\beta} + \frac{\sqrt{M}}{2\beta}(tanh_C(\sqrt{M}\eta) \pm \iota\sqrt{pq}sech_C(\sqrt{M}\eta))])e^{\iota(-kx+\omega t)}, \tag{4.33}$$

and

$$\psi_8(\eta) = 2\epsilon(\alpha - \delta k_2)(c_0 + \frac{2\beta c_0}{\mu}[-\frac{\mu}{2\beta} + \frac{\sqrt{M}}{2\beta}(tanh_C(\sqrt{M}\eta) \pm \iota\sqrt{pq}sech_C(\sqrt{M}\eta))])^2, \tag{4.34}$$

$$U_9(\eta) = c_0 + \frac{2\beta c_0}{\mu}[-\frac{\mu}{2\beta} + \frac{\sqrt{M}}{2\beta}(coth_C(\sqrt{M}\eta) \pm \sqrt{pq}csch_C(\sqrt{M}\eta))]. \tag{4.35}$$

The following solitary wave solutions for (1.2) are obtained with the aid of (4.1) and (4.6):

$$\phi_9(\eta) = (c_0 + \frac{2\beta c_0}{\mu}[-\frac{\mu}{2\beta} + \frac{\sqrt{M}}{2\beta}(coth_C(\sqrt{M}\eta) \pm \sqrt{pq}csch_C(\sqrt{-M}\eta))])e^{\iota(-kx+\omega t)}, \tag{4.36}$$

and

$$\psi_9(\eta) = 2\epsilon(\alpha - \delta k_2)(c_0 + \frac{2\beta c_0}{\mu}[-\frac{\mu}{2\beta} + \frac{\sqrt{M}}{2\beta}(coth_C(\sqrt{M}\eta) \pm \sqrt{pq}csch_C(\sqrt{M}\eta))])^2, \tag{4.37}$$

$$U_{10}(\eta) = c_0 + \frac{2\beta c_0}{\mu}[-\frac{\mu}{2\beta} + \frac{\sqrt{M}}{4\beta}(tanh_C(\frac{\sqrt{M}}{4}\eta) - coth_C(\frac{\sqrt{M}}{4}\eta))]. \tag{4.38}$$

The following solitary wave solutions for (1.2) are obtained with the aid of (4.1) and (4.6):

$$\phi_{10}(\eta) = (c_0 + \frac{2\beta c_0}{\mu}[-\frac{\mu}{2\beta} + \frac{\sqrt{M}}{4\beta}(tanh_C(\frac{\sqrt{M}}{4}\eta) - coth_C(\frac{\sqrt{M}}{4}\eta))])e^{\iota(-kx+\omega t)}, \tag{4.39}$$

and

$$\psi_{10}(\eta) = 2\epsilon(\alpha - \delta k_2)(c_0 + \frac{2\beta c_0}{\mu}[-\frac{\mu}{2\beta} + \frac{\sqrt{-M}}{4\beta}(tanh_C(\frac{\sqrt{M}}{4}\eta) - coth_C(\frac{\sqrt{M}}{4}\eta))])^2. \tag{4.40}$$

All the solutions of Family 2 are stable under the condition $M > 0$, ensuring their physical relevance and stability.

Family 3. When $\mu^2 = 4\varkappa\beta$, then

$$U_{11}(\eta) = c_0 + \frac{2\beta c_0}{\mu}[\frac{-2\varkappa(\mu\eta LnC + 2)}{\mu^2\eta LnC}]. \tag{4.41}$$

The following solitary wave solutions for (1.2) are obtained with the aid of (4.1) and (4.6):

$$\phi_{11}(\eta) = (c_0 + \frac{2\beta c_0}{\mu}[\frac{-2\varkappa(\mu\eta LnC + 2)}{\mu^2\eta LnC}])e^{\iota(-kx+\omega t)}, \tag{4.42}$$

and

$$\psi_{11}(\eta) = 2\epsilon(\alpha - \delta k_2)(c_0 + \frac{2\beta c_0}{\mu}[\frac{-2\varkappa(\mu\eta LnC + 2)}{\mu^2\eta LnC}])^2. \tag{4.43}$$

All the solutions of Family 3 are stable under the condition $\mu^2 = 4\varkappa\beta$, ensuring their physical relevance and stability.

Family 4. When $\mu \neq 0$ and $\varkappa = 0$, then

$$U_{12}(\eta) = c_0 + \frac{2\beta c_0}{\mu}[-\frac{p\mu}{\beta(cosh_C(\mu\eta) - sinh_C(\mu\eta) + p)}]. \tag{4.44}$$

The following solitary wave solutions for (1.2) are obtained with the aid of (4.1) and (4.6):

$$\phi_{12}(\eta) = (c_0 + \frac{2\beta c_0}{\mu}[-\frac{p\mu}{\beta(cosh_C(\mu\eta) - sinh_C(\mu\eta) + p)}])e^{\iota(-kx+\omega t)}, \tag{4.45}$$

and

$$\psi_{12}(\eta) = 2\epsilon(\alpha - \delta k_2)(c_0 + \frac{2\beta c_0}{\mu}[-\frac{p\mu}{\beta(cosh_C(\mu\eta) - sinh_C(\mu\eta) + p)}])^2, \tag{4.46}$$

$$U_{13}(\eta) = c_0 + \frac{2\beta c_0}{\mu}[-\frac{\mu(sinh_C(\mu\eta) + cosh_C(\mu\eta))}{\beta(sinh_C(\mu\eta) + cosh_C(\mu\eta) + q)}]. \tag{4.47}$$

The following solitary wave solutions for (1.2) are obtained with the aid of (4.1) and (4.6):

$$\phi_{13}(\eta) = (c_0 + \frac{2\beta c_0}{\mu}[-\frac{\mu(sinh_C(\mu\eta) + cosh_C(\mu\eta))}{\beta(sinh_C(\mu\eta) + cosh_C(\mu\eta) + q)}])e^{\iota(-kx+\omega t)}, \tag{4.48}$$

and

$$\psi_{13}(\eta) = 2\epsilon(\alpha - \delta k_2)(c_0 + \frac{2\beta c_0}{\mu}[-\frac{\mu(sinh_C(\mu\eta) + cosh_C(\mu\eta))}{\beta(sinh_C(\mu\eta) + cosh_C(\mu\eta) + q)}])^2. \tag{4.49}$$

All the solutions of Family 4 are stable under the conditions $\mu \neq 0$ and $\varkappa = 0$, ensuring their physical relevance and stability.

Family 5. When $\mu = \lambda, \beta = m\lambda$ $(m \neq 0)$, and $\varkappa = 0$, then

$$U_{14}(\eta) = c_0 + \frac{2\beta c_0}{\mu}[\frac{pC^{\lambda\eta}}{q - mpC^{\lambda\eta}}]. \tag{4.50}$$

The following solitary wave solutions for (1.2) are obtained with the aid of (4.1) and (4.6):

$$\phi_{14}(\eta) = (c_0 + \frac{2\beta c_0}{\mu}[\frac{pC^{\lambda\eta}}{q - mpC^{\lambda\eta}}])e^{\iota(-kx+\omega t)}, \tag{4.51}$$

and

$$\psi_{14}(\eta) = 2\epsilon(\alpha - \delta k_2)(c_0 + \frac{2\beta c_0}{\mu}[\frac{pC^{\lambda\eta}}{q - mpC^{\lambda\eta}}])^2. \tag{4.52}$$

All the solutions of Family 5 are stable under the conditions $\mu = \lambda$, $\beta = m\lambda$ $(m \neq 0)$, and $\varkappa = 0$, ensuring their physical relevance and stability.

We now have the following families of optical soliton solutions, assuming Case 2.

Family 6. When $M < 0$ and $\beta \neq 0$, then

$$U_{15}(\eta) = c_0 + \frac{2\varkappa c_0}{\mu}[-\frac{\mu}{2\beta} + \frac{\sqrt{-M}}{2\beta}tan_C(\frac{\sqrt{-M}}{2}\eta)]^{-1}. \tag{4.53}$$

The following solitary wave solutions for (1.2) are obtained with the aid of (4.1) and (4.6):

$$\phi_{15}(\eta) = (c_0 + \frac{2\varkappa c_0}{\mu}[-\frac{\mu}{2\beta} + \frac{\sqrt{-M}}{2\beta}tan_C(\frac{\sqrt{-M}}{2}\eta)]^{-1})e^{\iota(-kx+\omega t)}, \tag{4.54}$$

and

$$\psi_{15}(\eta) = 2\epsilon(\alpha - \delta k_2)(c_0 + \frac{2\varkappa c_0}{\mu}[-\frac{\mu}{2\beta} + \frac{\sqrt{-M}}{2\beta}tan_C(\frac{\sqrt{-M}}{2}\eta)]^{-1})^2, \tag{4.55}$$

$$U_{16}(\eta) = c_0 + \frac{2\varkappa c_0}{\mu}[-\frac{\mu}{2\beta} + \frac{\sqrt{-M}}{2\beta}cot_C(\frac{\sqrt{-M}}{2}\eta)]^{-1}. \tag{4.56}$$

The following solitary wave solutions for (1.2) are obtained with the aid of (4.1) and (4.6):

$$\phi_{16}(\eta) = (c_0 + \frac{2\varkappa c_0}{\mu}[-\frac{\mu}{2\beta} + \frac{\sqrt{-M}}{2\beta}cot_C(\frac{\sqrt{-M}}{2}\eta)]^{-1})e^{\iota(-kx+\omega t)}, \tag{4.57}$$

and

$$\psi_{16}(\eta) = 2\epsilon(\alpha - \delta k_2)(c_0 + \frac{2\varkappa c_0}{\mu}[-\frac{\mu}{2\beta} + \frac{\sqrt{-M}}{2\beta}cot_C(\frac{\sqrt{-M}}{2}\eta)]^{-1})^2, \tag{4.58}$$

$$U_{17}(\eta) = c_0 + \frac{2\varkappa c_0}{\mu}[-\frac{\mu}{2\beta} + \frac{\sqrt{-M}}{2\beta}(tan_C(\sqrt{-M}\eta) \pm \sqrt{pq}sec_C(\sqrt{-M}\eta))]^{-1}. \tag{4.59}$$

The following solitary wave solutions for (1.2) are obtained with the aid of (4.1) and (4.6):

$$\phi_{17}(\eta) = (c_0 + \frac{2\varkappa c_0}{\mu}[-\frac{\mu}{2\beta} + \frac{\sqrt{-M}}{2\beta}(tan_C(\sqrt{-M}\eta) \pm \sqrt{pq}sec_C(\sqrt{-M}\eta))]^{-1})e^{\iota(-kx+\omega t)}, \tag{4.60}$$

and

$$\psi_{17}(\eta) = 2\epsilon(\alpha - \delta k_2)(c_0 + \frac{2\varkappa c_0}{\mu}[-\frac{\mu}{2\beta} + \frac{\sqrt{-M}}{2\beta}(tan_C(\sqrt{-M}\eta) \pm \sqrt{pq}sec_C(\sqrt{-M}\eta))]^{-1})^2, \tag{4.61}$$

$$U_{18}(\eta) = c_0 + \frac{2\varkappa c_0}{\mu}[-\frac{\mu}{2\beta} + \frac{\sqrt{-M}}{2\beta}(cot_C(\sqrt{-M}\eta) \pm \sqrt{pq}csc_C(\sqrt{-M}\eta))]^{-1}. \tag{4.62}$$

The following solitary wave solutions for (1.2) are obtained with the aid of (4.1) and (4.6):

$$\phi_{18}(\eta) = (c_0 + \frac{2\varkappa c_0}{\mu}[-\frac{\mu}{2\beta} + \frac{\sqrt{-M}}{2\beta}(cot_C(\sqrt{-M}\eta) \pm \sqrt{pq}csc_C(\sqrt{-M}\eta))]^{-1})e^{\iota(-kx+\omega t)}, \tag{4.63}$$

and

$$\psi_{18}(\eta) = 2\epsilon(\alpha - \delta k_2)(c_0 + \frac{2\varkappa c_0}{\mu}[-\frac{\mu}{2\beta} + \frac{\sqrt{-M}}{2\beta}(cot_C(\sqrt{-M}\eta) \pm \sqrt{pq}csc_C(\sqrt{-M}\eta))]^{-1})^2, \tag{4.64}$$

$$U_{19}(\eta) = c_0 + \frac{2\varkappa c_0}{\mu}[-\frac{\mu}{2\beta} + \frac{\sqrt{-M}}{4\beta}(tan_C(\frac{\sqrt{-M}}{4}\eta) - cot_C(\frac{\sqrt{-M}}{4}\eta))]^{-1}. \tag{4.65}$$

The following solitary wave solutions for (1.2) are obtained with the aid of (4.1) and (4.6):

$$\phi_{19}(\eta) = (c_0 + \frac{2\varkappa c_0}{\mu}[-\frac{\mu}{2\beta} + \frac{\sqrt{-M}}{4\beta}(tan_C(\frac{\sqrt{-M}}{4}\eta) - cot_C(\frac{\sqrt{-M}}{4}\eta))]^{-1})e^{\iota(-kx+\omega t)}, \tag{4.66}$$

and

$$\psi_{19}(\eta) = 2\epsilon(\alpha - \delta k_2)(c_0 + \frac{2\varkappa c_0}{\mu}[-\frac{\mu}{2\beta} + \frac{\sqrt{-M}}{4\beta}(tan_C(\frac{\sqrt{-M}}{4}\eta) - cot_C(\frac{\sqrt{-M}}{4}\eta))]^{-1})^2. \tag{4.67}$$

All the solutions of Family 6 are stable under the condition $M < 0$, ensuring their physical relevance and stability.

Family 7. When $M > 0$ and $\beta \neq 0$, then

$$U_{20}(\eta) = c_0 + \frac{2\varkappa c_0}{\mu}[-\frac{\mu}{2\beta} + \frac{\sqrt{M}}{2\beta}tanh_C(\frac{\sqrt{M}}{2}\eta)]^{-1}. \tag{4.68}$$

The following solitary wave solutions for (1.2) are obtained with the aid of (4.1) and (4.6):

$$\phi_{20}(\eta) = (c_0 + \frac{2\varkappa c_0}{\mu}[-\frac{\mu}{2\beta} + \frac{\sqrt{M}}{2\beta}tanh_C(\frac{\sqrt{M}}{2}\eta)]^{-1})e^{\iota(-kx+\omega t)}, \tag{4.69}$$

and

$$\psi_{20}(\eta) = 2\epsilon(\alpha - \delta k_2)(c_0 + \frac{2\varkappa c_0}{\mu}[-\frac{\mu}{2\beta} + \frac{\sqrt{M}}{2\beta}tanh_C(\frac{\sqrt{M}}{2}\eta)]^{-1})^2, \tag{4.70}$$

$$U_{21}(\eta) = c_0 + \frac{2\varkappa c_0}{\mu}[-\frac{\mu}{2\beta} + \frac{\sqrt{M}}{2\beta}coth_C(\frac{\sqrt{M}}{2}\eta)]^{-1}. \tag{4.71}$$

The following solitary wave solutions for (1.2) are obtained with the aid of (4.1) and (4.6):

$$\phi_{21}(\eta) = (c_0 + \frac{2\varkappa c_0}{\mu}[-\frac{\mu}{2\beta} + \frac{\sqrt{M}}{2\beta}coth_C(\frac{\sqrt{M}}{2}\eta)]^{-1})e^{\iota(-kx+\omega t)}, \tag{4.72}$$

and

$$\psi_{21}(\eta) = 2\epsilon(\alpha - \delta k_2)(c_0 + \frac{2\varkappa c_0}{\mu}[-\frac{\mu}{2\beta} + \frac{\sqrt{M}}{2\beta}coth_C(\frac{\sqrt{M}}{2}\eta)]^{-1})^2, \tag{4.73}$$

$$U_{22}(\eta) = c_0 + \frac{2\varkappa c_0}{\mu}[-\frac{\mu}{2\beta} + \frac{\sqrt{M}}{2\beta}(tanh_C(\sqrt{M}\eta) \pm \iota\sqrt{pq}sech_C(\sqrt{M}\eta))]^{-1}. \tag{4.74}$$

The following solitary wave solutions for (1.2) are obtained with the aid of (4.1) and (4.6):

$$\phi_{22}(\eta) = (c_0 + \frac{2\varkappa c_0}{\mu}[-\frac{\mu}{2\beta} + \frac{\sqrt{M}}{2\beta}(tanh_C(\sqrt{M}\eta) \pm \iota\sqrt{pq}sech_C(\sqrt{M}\eta))]^{-1})e^{\iota(-kx+\omega t)}, \tag{4.75}$$

and

$$\psi_{22}(\eta) = 2\epsilon(\alpha - \delta k_2)(c_0 + \frac{2\varkappa c_0}{\mu}[-\frac{\mu}{2\beta} + \frac{\sqrt{M}}{2\beta}(tanh_C(\sqrt{M}\eta) \pm \iota\sqrt{pq}sech_C(\sqrt{M}\eta))]^{-1})^2, \tag{4.76}$$

$$U_{23}(\eta) = c_0 + \frac{2\varkappa c_0}{\mu}[-\frac{\mu}{2\beta} + \frac{\sqrt{M}}{2\beta}(coth_C(\sqrt{M}\eta) \pm \sqrt{pq}csch_C(\sqrt{M}\eta))]^{-1}. \tag{4.77}$$

The following solitary wave solutions for (1.2) are obtained with the aid of (4.1) and (4.6):

$$\phi_{23}(\eta) = (c_0 + \frac{2\varkappa c_0}{\mu}[-\frac{\mu}{2\beta} + \frac{\sqrt{M}}{2\beta}(coth_C(\sqrt{M}\eta) \pm \sqrt{pq}csch_C(\sqrt{-M}\eta))]^{-1})e^{\iota(-kx+\omega t)}, \tag{4.78}$$

and

$$\psi_{23}(\eta) = 2\epsilon(\alpha - \delta k_2)(c_0 + \frac{2\varkappa c_0}{\mu}[-\frac{\mu}{2\beta} + \frac{\sqrt{M}}{2\beta}(coth_C(\sqrt{M}\eta) \pm \sqrt{pq}csch_C(\sqrt{M}\eta))]^{-1})^2, \tag{4.79}$$

$$U_{24}(\eta) = c_0 + \frac{2\varkappa c_0}{\mu}[-\frac{\mu}{2\beta} + \frac{\sqrt{M}}{4\beta}(tanh_C(\frac{\sqrt{M}}{4}\eta) - coth_C(\frac{\sqrt{M}}{4}\eta))]^{-1}. \tag{4.80}$$

The following solitary wave solutions for (1.2) are obtained with the aid of (4.1) and (4.6):

$$\phi_{24}(\eta) = (c_0 + \frac{2\varkappa c_0}{\mu}[-\frac{\mu}{2\beta} + \frac{\sqrt{M}}{4\beta}(tanh_C(\frac{\sqrt{M}}{4}\eta) - coth_C(\frac{\sqrt{M}}{4}\eta))]^{-1})e^{\iota(-kx+\omega t)}, \tag{4.81}$$

and

$$\psi_{24}(\eta) = 2\epsilon(\alpha - \delta k_2)(c_0 + \frac{2\varkappa c_0}{\mu}[-\frac{\mu}{2\beta} + \frac{\sqrt{-M}}{4\beta}(tanh_C(\frac{\sqrt{M}}{4}\eta) - coth_C(\frac{\sqrt{M}}{4}\eta))]^{-1})^2. \tag{4.82}$$

All the solutions of Family 7 are stable under the condition $M > 0$, ensuring their physical relevance and stability.

Family 8. When $\mu^2 = 4\varkappa\beta$, then

$$U_{25}(\eta) = c_0 + \frac{2\varkappa c_0}{\mu}[\frac{-2\varkappa(\mu\eta LnC + 2)}{\mu^2\eta LnC}]^{-1}. \tag{4.83}$$

The following solitary wave solutions for (1.2) are obtained with the aid of (4.1) and (4.6):

$$\phi_{25}(\eta) = (c_0 + \frac{2\varkappa c_0}{\mu}[\frac{-2\varkappa(\mu\eta LnC + 2)}{\mu^2\eta LnC}]^{-1})e^{\iota(-kx+\omega t)}, \tag{4.84}$$

and

$$\psi_{25}(\eta) = 2\epsilon(\alpha - \delta k_2)(c_0 + \frac{2\varkappa c_0}{\mu}[\frac{-2\varkappa(\mu\eta LnC + 2)}{\mu^2\eta LnC}]^{-1})^2. \tag{4.85}$$

All the solutions of Family 8 are stable under the condition $\mu^2 = 4\varkappa\beta$, ensuring their physical relevance and stability.

4.2. Application of the new Kudryashov method

For $\Theta = 1$, Eq (3.8) reduces to the form:

$$U(\xi) = f_0 + f_1 H(\xi). \tag{4.86}$$

Plugging the above solution with (3.7) into (4.7) and setting the coefficients of $H_i(\xi)$ $(i = 0, 1, \dots)$ to zero, the following system is acquired:

$$\begin{aligned}
(H(\eta))^0 &: (-2k\alpha c_0 + k^2\alpha\delta c_0 + 2\alpha\gamma\delta\epsilon c_0^3 - c_0k_2 + 2k\delta c_0k_2 - k^2\delta^2c_0k_2 - 2\gamma\delta^2\epsilon c_0^3k_2) = 0,\\
(H(\eta))^1 &: (-2k\alpha c_1 + k^2\alpha\delta c_1 + \alpha\delta\sigma^2c_1 + 6\alpha\gamma\delta\epsilon c_0^2c_1 - c_1k_2 + 2k\delta c_1k_2 - k^2\delta^2c_1k_2 - \delta^2\sigma^2c_1k_2\\
&\quad -6\gamma\delta^2\epsilon c_0^2c_1k_2) = 0,\\
(H(\eta))^2 &: (6\alpha\gamma\delta\epsilon c_0c_1^2 - 6\gamma\delta^2\epsilon c_0c_1^2k_2) = 0,\\
(H(\eta))^3 &: (2m\alpha\delta\sigma^2c_1 + 2\alpha\gamma\delta\epsilon c_1^2 - 2m\delta^2\sigma^2c_1k_2 - 2\gamma\delta^2\epsilon c_1^3k_2) = 0.
\end{aligned}$$

By solving this system of equations, we obtain the following solution:

$$c_0 = 0,\ \alpha = \frac{(1 - 2k\delta + k^2\delta^2 + \delta^2\sigma^2)k_2)}{(-2k + k^2\delta + \delta\sigma^2)},\ m = -\frac{(\gamma\epsilon c_1^2)}{\sigma^2}. \tag{4.87}$$

Utilizing Eqs (4.86) and (4.87), the following solutions are required:

$$U_1(\xi) = c_1(\frac{2\nu B}{B^2e^{\nu\sigma\xi} - me^{-\nu\sigma\xi}})e^{i(-kx+\omega t)}. \tag{4.88}$$

The hyperbolic solution of Eq (4.88) takes the following form:

$$U_2(\xi) = c_1(\frac{2\nu B}{(B^2 - m)cosh(\sigma\xi) + (B^2 + m)sinh(\sigma\xi)})e^{i(-kx+\omega t)}. \tag{4.89}$$

Plugging $m = -B^2$ in solutions (4.89), the following solutions are constructed:

$$U_3(\xi) = \frac{c_1\nu}{B}sech(\sigma\xi)e^{i(-kx+\omega t)}. \tag{4.90}$$

Plugging $m = B^2$ in solutions (4.89), the following solutions are constructed:

$$U_4(\xi) = \frac{c_1\nu}{B}csch(\sigma\xi)e^{i(-kx+\omega t)}. \tag{4.91}$$

5. Findings and analysis

The results of this study reveal much about the fractional-order Akbota equation, on the grounds of which a lot of important system features were observed in the light of graphs and traveling wave solutions. Solutions illustrated that the fractional Akobta equation has solitary waves and hyperbolic solutions of the high order. The graphical results clearly demonstrate how variations in the fractional-order ρ affect wave profiles, highlighting phenomena such as sharper peaks, oscillations, and singularities that reflect realistic signal behaviors in telecommunications.

In order to explain the wave patterns, we employ three-dimensional (3D) and two-dimensional (2D) graphs. It might also be noted that by varying the values assigned to the variables in the equations, one can obtain a great number of graphs, which description contains certain specific features of the answer. To the same answers, graphic depictions including 3D and 2D are used so that the flow of waves may be easily understood. To investigate the behavior of the solutions, we have represented the two-dimensional and three-dimensional plots for soliton solutions of the given Eqs

(4.12), (4.18), (4.27), (4.54), (4.57), (4.60), (4.63), (4.66), and (4.90) with different fractional-order values in Figures 1–9. Each figure illustrates how different solution types-singular, oscillatory, periodic, bright, dark, and breather solitons-correspond to real-world signal behaviors in optical fibers, such as amplification, distortion, and instability. The fractional-order ρ significantly influences these dynamics: lower values yield smoother signals, while higher values produce sharper, more unstable waveforms. These insights help bridge the mathematical results with practical phenomena in fiber-optic communication systems.

Thus, this paper proves that the mEDAM and new Kudryashov method can be efficient and versatile approaches to solving elaborate models in mathematics. The comparison of these methods with other methods is given in Table 1.

Table 1. Comparison of the mEDAM with other soliton solution methods.

Criteria	**Our Method**	**Hirota Bilinear Method**	**Variational Method**	**Tanh Method**
Applicability to fractional equations	Well-suited; easily handles conformable derivatives	Difficult to apply directly to fractional forms	Less effective for fractional derivatives	Can be extended, but with limitations in fractional context
Equation type	Reduces PDE to ODE for solution	Requires bilinear form of PDE	Requires construction of a trial Lagrangian	Converts ODE into algebraic form
Solution diversity	Generates wide variety (bright, dark, periodic-singular, breather)	Mostly soliton-type (bright/dark)	Usually yields approximate solutions	Often yields single-soliton solutions
Complexity	Moderate	High (due to bilinear transformation)	High (requires functional setup)	Low to moderate
Stability remarks	Allows condition-based stability discussion (e.g., $M > 0$)	Less emphasis on parameter-driven stability	Stability linked to variational conditions	Limited insight into stability
Novelty in this study	Newly applied to fractional Akbota system	Not applied to Akbota in fractional setting	Not applied to current system	Commonly used in classical systems

In the existing literature, methods such as the Sardar sub-equation method, exp-function method, and the generalized Kudryashov method have been applied to nonlinear equations. However, the mEDAM and the new Kudryashov approach employed in this work have not been previously applied to the fractional Akbota equation, highlighting the novelty and originality of this study.

It has been adopted to several physical systems, which make the approach quite practical for

understanding the behavior of dispersive and nonlinear physical systems. Analysis of the results obtained by this approach can provide us with useful information on the behavior of the fractional Akobta system and phenomena connected with it, and hence, a profound impact on our understanding of the fundamental laws in physics can be provided.

Figures 1 exhibits a singular and oscillatory behavior. It is not periodic but demonstrates localized sharp variations, similar to resonance phenomena in telecommunication systems. The selection of visualization encompasses 3D and 2D plots at different values of ρ, particularly $\rho = 0.79$, $\rho = 0.89$, and $\rho = 0.99$. At $\rho = 0.79$ (Figure 1(a)), the function exhibits moderate oscillatory behavior, resembling a stable system response with controlled variations. At $\rho = 0.89$ (Figure 1(b)), the oscillations intensify, and peaks become sharper, indicating increased signal fluctuations. At $\rho = 0.99$ (Figure 1(c)), the function experiences significant amplification, with sharp transitions and steep peaks, suggesting increased sensitivity. A 2D graph compares the function for different values of ρ using different colors (blue for $\rho = 0.79$, green for $\rho = 0.89$, and red for $\rho = 0.99$). As ρ increases, the system becomes more sensitive to small changes, similar to high-frequency filtering effects in signal processing. Figure 1 represents resonance or high-sensitivity points in the system where signal amplitudes may change rapidly. This behavior is useful for identifying instability thresholds, such as in nonlinear amplifiers or dispersion compensation schemes. Engineers can design safeguards or stabilizing techniques by analyzing where such sudden amplifications may occur.

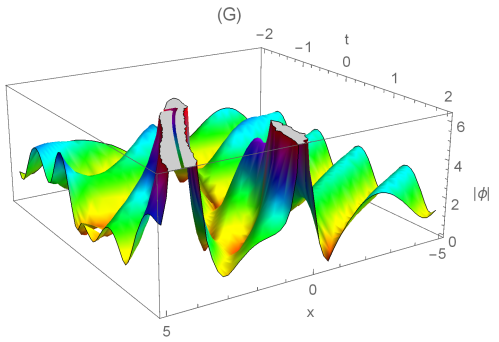

(a) 3D depiction at $\rho = 0.79$

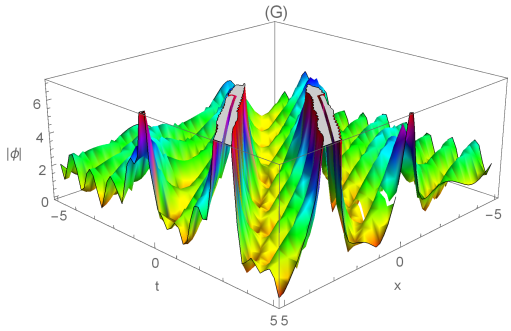

(b) 3D depiction at $\rho = 0.89$

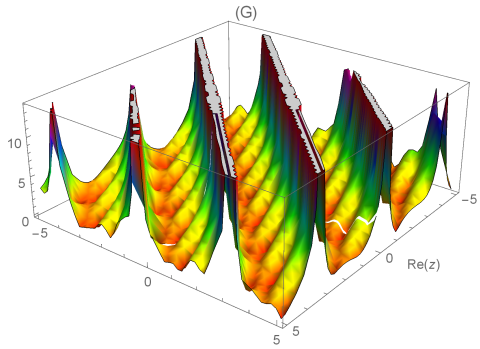

(c) 3D depiction at $\rho = 0.99$

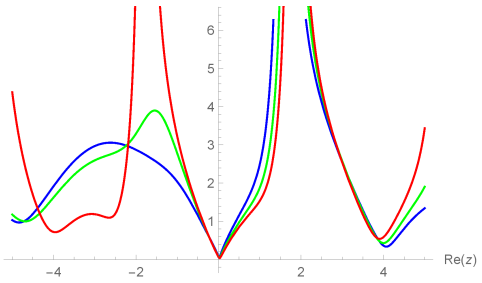

(d) 2D depiction at ____ ($\rho = 0.79$), ____ ($\rho = 0.89$), ____ ($\rho = 0.99$)

Figure 1. The effect of fractional order in two- and three-dimensional models for a solution (4.12) with $\mu = 1$, $\xi = 2$, $\beta = 1$, $\delta = 2$, $k_2 = 2$, $k = 1.5$, $c_0 = 1$, $\gamma = 2$, $C = e$.

Figure 2 exhibits singular and non-periodic behavior with strong peaks. The selection of visualization encompasses 3D and 2D plots at different values of ρ, particularly $\rho = 0.79$, $\rho = 0.89$, and $\rho = 0.99$. At $\rho = 0.79$ (Figure 2(a)), the function shows structured oscillations with a stable pattern. At $\rho = 0.89$ (Figure 2(b)), the function exhibits sharper peaks, indicating increased variations. At $\rho = 0.99$ (Figure 2(c)), the oscillations are significantly amplified, with extreme peaks and deep valleys. This is analogous to signal distortion in high-frequency communication, where making ρ larger can be viewed as a system becoming more sensitive to signal or noise variations. A 2D plot provides comparative insight into the function for different values of ρ employing different colors: blue for $\rho = 0.79$, green for $\rho = 0.89$, and red for $\rho = 0.99$. The increasing sharpness signifies that higher ρ produces stronger fluctuations in the signal, and this affects stability. The presence of singularities illustrates an impulse-like response, which is of utmost significance in designing error-correcting codes and signal restoration techniques. Figure 2 mimics repeated disturbances or signal distortion patterns in nonlinear media. Periodic singularities are analogous to jitter effects or multipath reflections in optical fibers. Understanding these patterns helps in designing filters or coding strategies that mitigate recurring distortions during transmission.

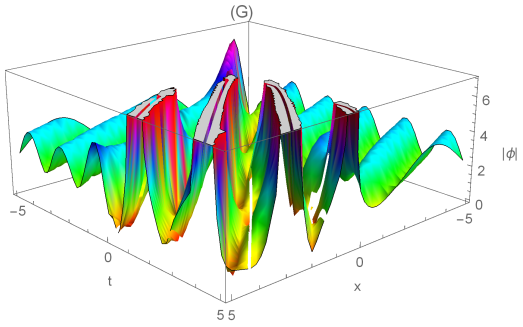

(a) 3D depiction at $\rho = 0.79$

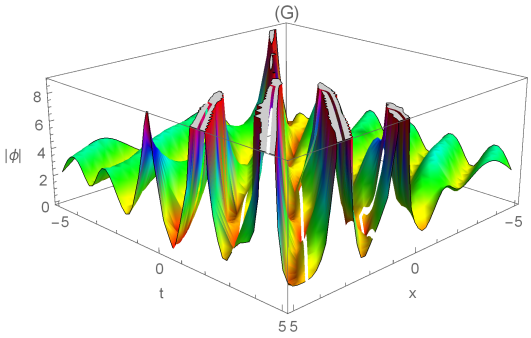

(b) 3D depiction at $\rho = 0.89$

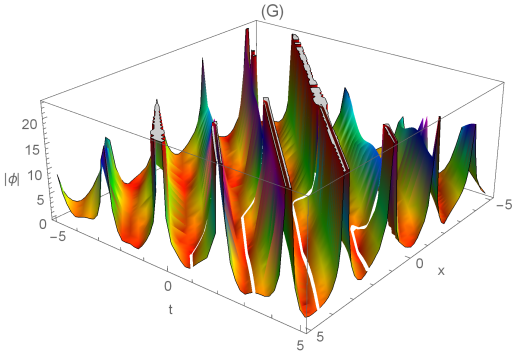

(c) 3D depiction at $\rho = 0.99$

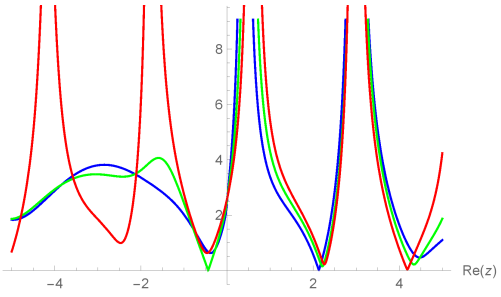

(d) 2D depiction at ___ ($\rho = 0.79$), ___ ($\rho = 0.89$), ___ ($\rho = 0.99$)

Figure 2. The effect of fractional order in two- and three-dimensional models for a solution (4.18) with $\mu = 1$, $\xi = 1$, $\beta = 1$, $\delta = 1$, $k_2 = 1$, $k = 1.5$, $c_0 = 1$, $c = d = 1$, $\gamma = 1$, $C = e$.

Figure 3 illustrates dark soliton behavior, which is characterized by localized dips in intensity rather than sharp peaks. This type of waveform is crucial in modeling signal dips or intensity drops in optical fiber communication, often used to represent stable, non-singular pulse propagation. The figure presents both 3D and 2D plots for different values of the fractional order $\rho = 0.79$, $\rho = 0.89$, and $\rho = 0.99$. At $\rho = 0.79$ (Figure 3(a)), the waveform exhibits a smooth and broad intensity dip, representing stable and low-distortion dark soliton. This reflects relatively low nonlinearity in the system, with minimal impact on signal shape. At $\rho = 0.89$ (Figure 3(b)), the depth of the soliton dip increases, and its width narrows, indicating a sharper localized drop in intensity. This suggests stronger nonlinear effects and more distinct pulse shaping. At $\rho = 0.99$ (Figure 3(c)), the dip becomes even steeper and more pronounced, resembling the behavior of high-contrast dark solitons. This reflects enhanced dispersion and stronger phase shifts, typical in high-order nonlinear systems. The 2D plot overlays the soliton profiles for each ρ using different colors for comparison. As ρ increases, the soliton becomes narrower and deeper, showcasing the effect of the fractional order on wave steepness and localization. This behavior is particularly relevant in fiber optic systems, where dark solitons offer advantages such as robustness against perturbations and lower sensitivity to noise, making them suitable for long-distance, high-capacity signal transmission. Figure 3 is used in optical switching and intensity-based logic gates. Dark solitons are dips in light intensity and are less sensitive to dispersion, making them robust for long-distance data transmission. They are also useful in WDM (wavelength-division multiplexing) systems due to their stability across channels.

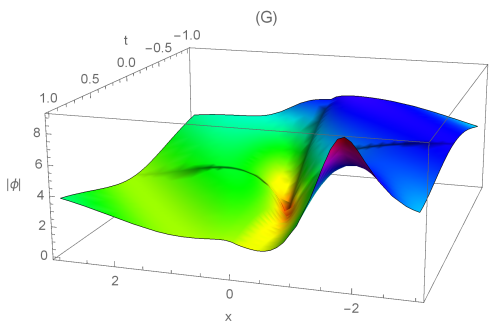

(a) 3D depiction at $\rho = 0.79$

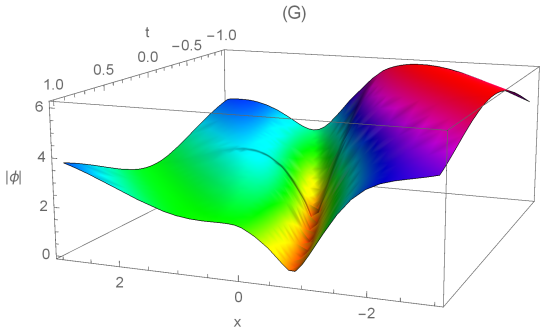

(b) 3D depiction at $\rho = 0.89$

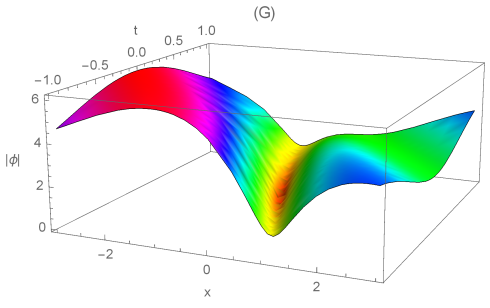

(c) 3D depiction at $\rho = 0.99$

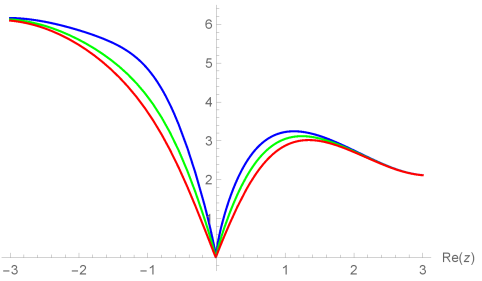

(d) 2D depiction at ___ ($\rho = 0.79$), ___ ($\rho = 0.89$), ___ ($\rho = 0.99$)

Figure 3. The effect of fractional order in two- and three-dimensional models for a solution (4.27) with $\mu = 0.5$, $\xi = -1$, $\beta = 1$, $\delta = 2$, $k_2 = -1$, $k = 1$, $c_0 = 1$, $\gamma = 1$, $C = e$.

Figures 4 exhibits a singular and oscillatory behavior. It is not periodic but demonstrates localized sharp variations, similar to resonance phenomena in telecommunication systems. The selection of visualization encompasses 3D and 2D plots at different values of ρ, particularly $\rho = 0.79$, $\rho = 0.89$, and $\rho = 0.99$. At $\rho = 0.79$ (Figure 4(a)), the function exhibits moderate oscillatory behavior, resembling a stable system response with controlled variations. At $\rho = 0.89$ (Figure 4(b)), the oscillations intensify, and peaks become sharper, indicating increased signal fluctuations. At $\rho = 0.99$ (Figure 4(c)), the function experiences significant amplification, with sharp transitions and steep peaks, suggesting increased sensitivity. The 2D graph compares the function for different values of ρ using different colors (blue for $\rho = 0.79$, green for $\rho = 0.89$, and red for $\rho = 0.99$). As ρ increases, the system becomes more sensitive to small changes, similar to high-frequency filtering effects in signal processing. Figure 4 illustrates energy localization at specific points. This is important in designing optical power limiters or fault detection systems, where sudden spikes indicate a breach in normal signal flow. It can also aid in modulator calibration under nonlinear loads.

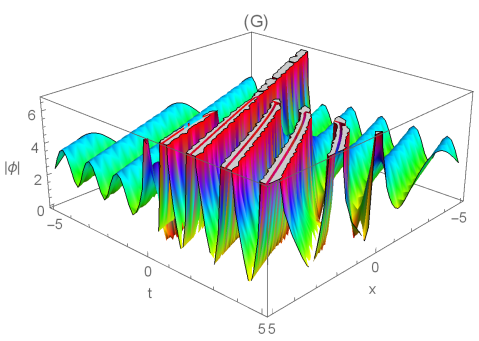

(a) 3D depiction at $\rho = 0.79$

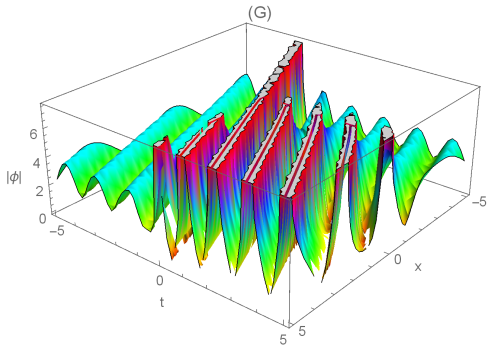

(b) 3D depiction at $\rho = 0.89$

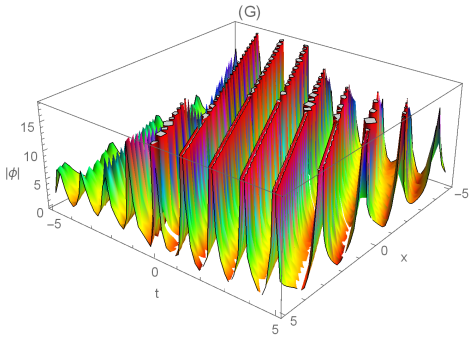

(c) 3D depiction at $\rho = 0.99$

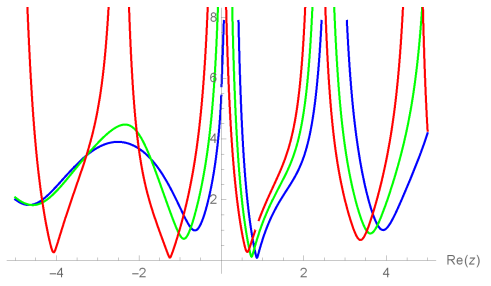

(d) 2D depiction at ___ ($\rho = 0.79$), ___ ($\rho = 0.89$), ___ ($\rho = 0.99$)

Figure 4. The effect of fractional order in two- and three-dimensional models for a solution (4.54) with $\mu = -0.5$, $\xi = -0.9$, $\beta = 1.5$, $\delta = 0.6$, $k_2 = -1.5$, $k = -1.5$, $c_0 = 0.8$, $\gamma = 2$, $C = e$.

Figure 5 illustrates singular behavior with steep peaks. This indicates that it might be used to represent resonance phenomena or impulse responses in communication channels. The fact that there are singularities implies that, in some places, the signal is amplified suddenly, which is a key determinant in avoiding instability in communication networks. The selection of visualization encompasses 3D and 2D plots at different values of ρ, particularly $\rho = 0.79$, $\rho = 0.89$, and $\rho = 0.99$. At $\rho = 0.79$ (Figure 5(a)), the function demonstrates smooth variations with a moderate peak and valley, resembling a stable signal response. At $\rho = 0.89$ (Figure 5(b)), the peak increases, and the function shows sharper variations, indicating a stronger response to changes in input. At $\rho = 0.99$ (Figure 5(c)), the function has significantly steeper peaks and more pronounced changes, suggesting an amplification effect often seen in high-gain systems. This behavior is similar to how signals react under different attenuation and amplification conditions, where a higher fractional order ρ can represent increased signal sharpness and potential instability in filters or modulation schemes. The 2D plot provides a comparative view of the function for different values of ρ. Figure 5 helps simulate abrupt signal phase changes or phase jitter scenarios. These insights are applicable in coherent communication systems, where managing phase noise is critical for performance. Understanding such singular transitions improves carrier synchronization and demodulation fidelity.

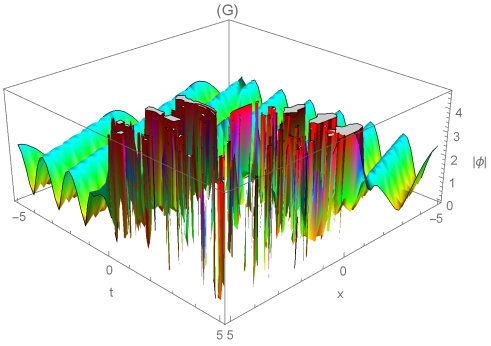

(a) 3D depiction at $\rho = 0.79$

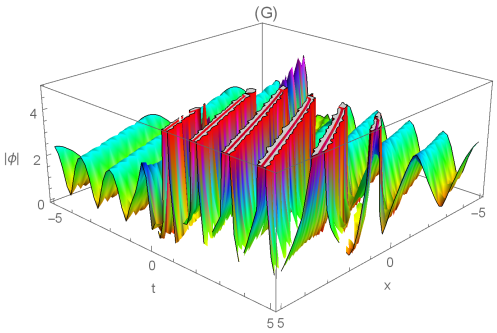

(b) 3D depiction at $\rho = 0.89$

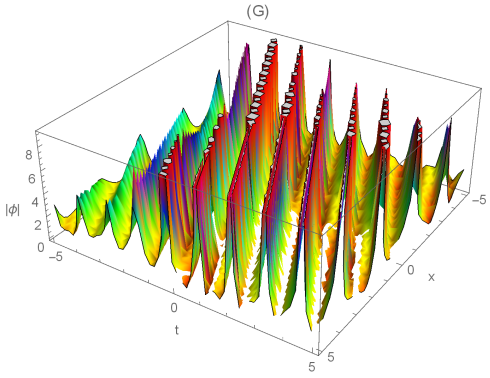

(c) 3D depiction at $\rho = 0.99$

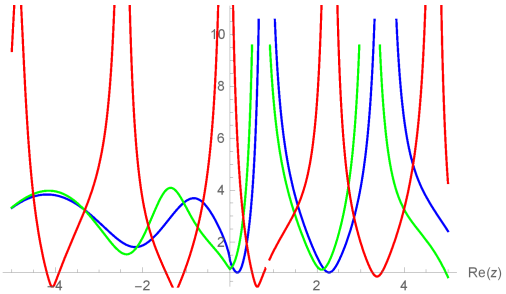

(d) 2D depiction at ___ ($\rho = 0.79$), ___ ($\rho = 0.89$), ___ ($\rho = 0.99$)

Figure 5. The effect of fractional order in two- and three-dimensional models for a solution (4.57) with $\mu = 1$, $\xi = 2$, $\beta = 1$, $\delta = 2$, $k_2 = 2$, $k = 1.5$, $c_0 = 1$, $\gamma = 2$, $C = e$.

The diagrams in Figures 6 and 7 highlight the periodic solutions at different values of ρ, particularly $\rho = 0.79$, $\rho = 0.89$, and $\rho = 0.99$. Periodic solitons facilitate signal timing stability and diminish the probability of errors in high-speed data streams by delivering consistent, repetitive waveforms. The function resembles signals that undergo modulation, where frequency components change over time. The peaks and singularities could represent signal amplification or interference in a telecommunication channel. The dependence on ρ suggests a fractional differential system, common in signal processing for modeling complex behavior. The 2D plot shows the comparison for different values of ρ. The curves show non-uniform behavior. Figure 6 models modulated signals used in dense wavelength division multiplexing (DWDM) and phase-shift keying (PSK) systems. The periodicity ensures consistent signal shape, helping in timing recovery circuits and clock synchronization mechanisms in receivers. Figure 7 is useful in advanced signal modulation schemes, such as QAM (quadrature amplitude modulation), where both amplitude and phase vary. The mixed periodic and singular traits simulate interference patterns from crosstalk, aiding in error correction algorithm development.

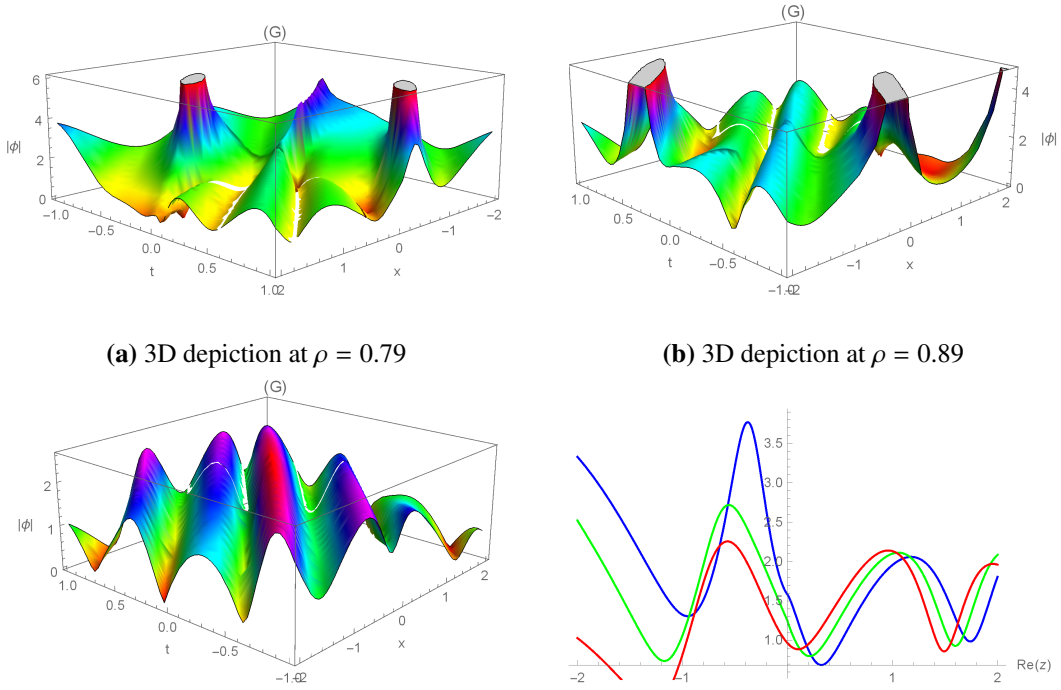

(a) 3D depiction at $\rho = 0.79$

(b) 3D depiction at $\rho = 0.89$

(c) 3D depiction at $\rho = 0.99$

(d) 2D depiction at ____ ($\rho = 0.79$), ____ ($\rho = 0.89$), ____ ($\rho = 0.99$)

Figure 6. The effect of fractional order in two- and three-dimensional models for a solution (4.60) with $\mu = 1, \xi = 2, \beta = 2, \delta = 2, k_2 = 2, k = 1.5, c = 2\,d = 3\,c_0 = 1, \gamma = 2, C = e$.

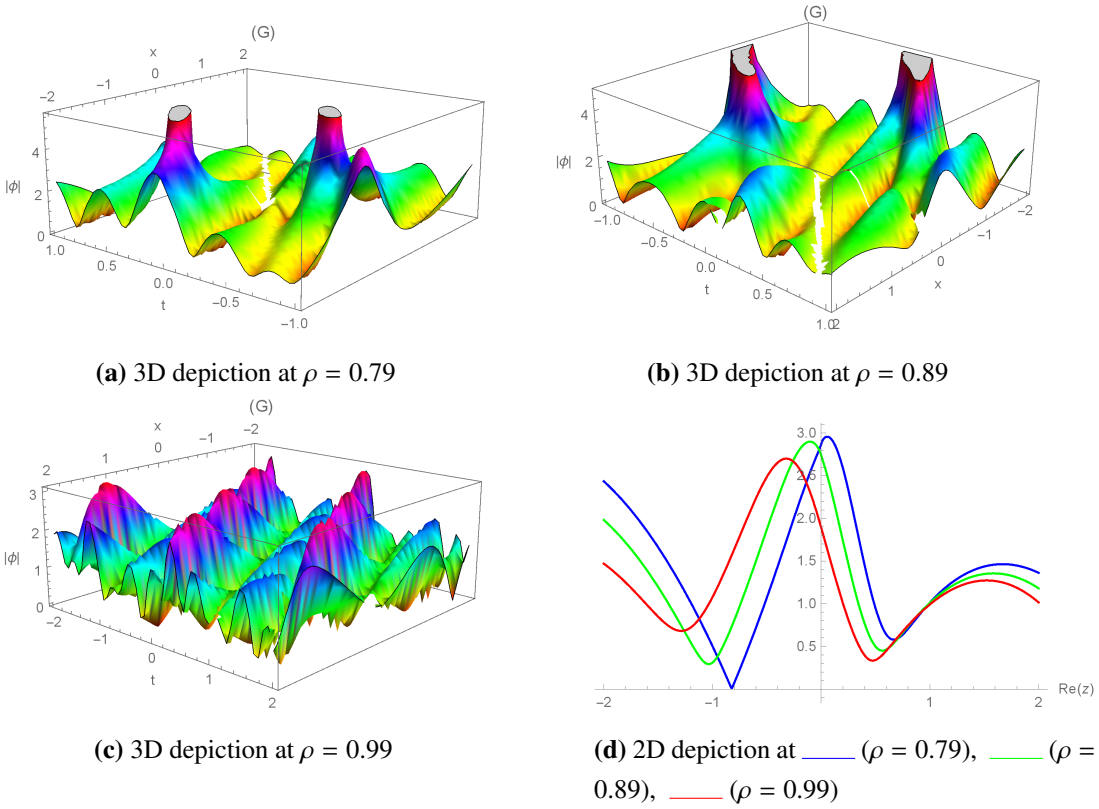

(a) 3D depiction at $\rho = 0.79$

(b) 3D depiction at $\rho = 0.89$

(c) 3D depiction at $\rho = 0.99$

(d) 2D depiction at ——— ($\rho = 0.79$), ——— ($\rho = 0.89$), ——— ($\rho = 0.99$)

Figure 7. The effect of fractional order in two- and three-dimensional models for a solution (4.63) with $\mu = 1$, $\xi = 1$, $\beta = 1$, $\delta = 1$, $k_2 = 2$, $k = 1.5$, $c_0 = 1$, $\gamma = 1$, $c = d = 1$, $C = e$.

The visualization of Figure 8 represents the breather soliton solution at independent values of ρ, particularly $\rho = 0.79$, $\rho = 0.89$, and $\rho = 0.99$. Breather solitons represent optical pulses with a constant amplitude throughout their propagation in optical fibers. The fractional-order ρ significantly affects the function's oscillatory nature, which may be useful in designing adaptive signal processing techniques. The 2D plot shows the comparison at different values of ρ. The function resembles signals that undergo modulation, where frequency components change over time. Figure 8 models pulse packets that breathe (oscillate) during propagation, ideal for ultra-short pulse communication and adaptive gain amplifiers. Their stable but dynamic structure helps optimize optical time-domain reflectometry (OTDR) and nonlinear pulse shaping.

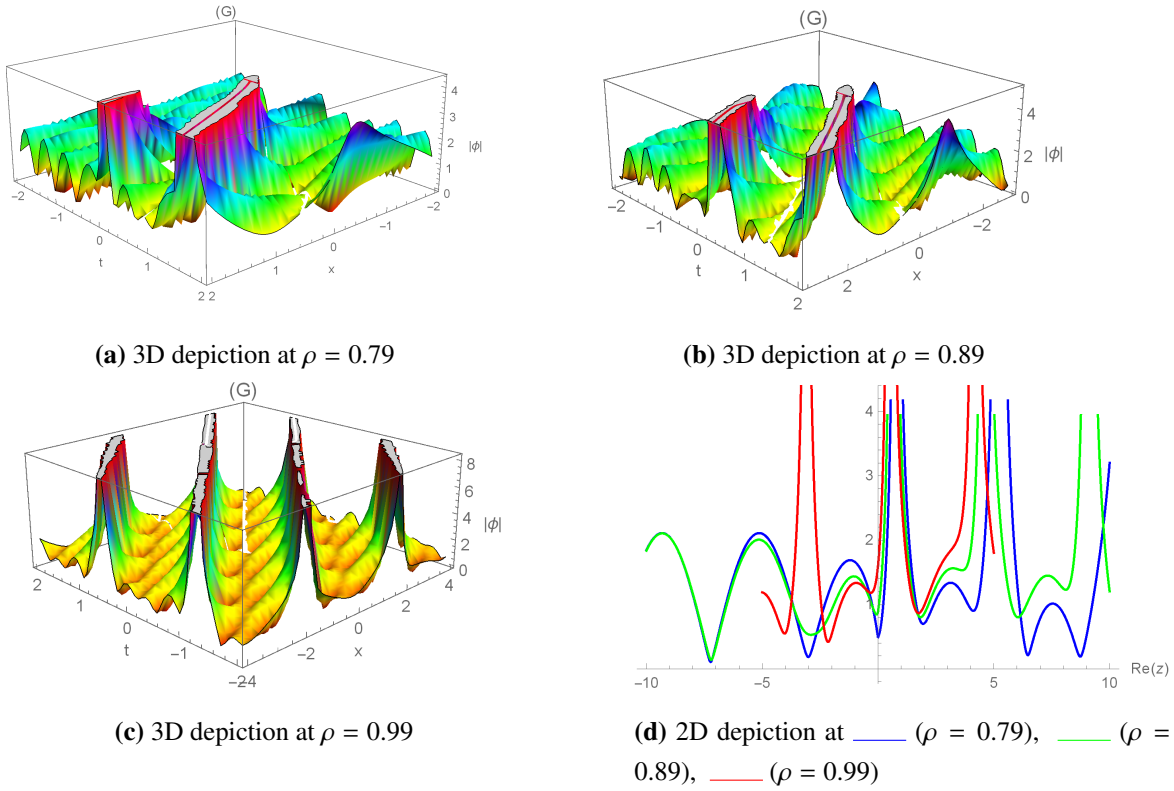

(a) 3D depiction at $\rho = 0.79$

(b) 3D depiction at $\rho = 0.89$

(c) 3D depiction at $\rho = 0.99$

(d) 2D depiction at ____ ($\rho = 0.79$), ____ ($\rho = 0.89$), ____ ($\rho = 0.99$)

Figure 8. The effect of fractional order in two- and three-dimensional models for a solution (4.66) with $\mu = 1$, $\xi = 2$, $\beta = 1$, $\delta = 2$, $k_2 = 2$, $k = 1.5$, $c_0 = 1$, $\gamma = 2$, $C = e$.

Figure 9 presents the effect of the fractional-order ρ on the solution derived from Eq (4.90), showcasing a bright soliton structure. Bright solitons are characterized by localized peaks in the wave profile and are commonly used to represent signal amplification or energy concentration in nonlinear optical systems. The visualization includes both 3D and 2D plots for three distinct values of $\rho = 0.79$, $\rho = 0.89$, and $\rho = 0.99$. At $\rho = 0.79$ (Figure 9(a)), the function displays a relatively broad and smooth peak, representing a gentle and stable energy packet. This behavior suggests minimal nonlinearity and dispersion in the system, conducive to low-distortion signal propagation. At $\rho = 0.89$ (Figure 9(b)), the peak becomes narrower and more pronounced, indicating an increase in wave intensity and tighter energy localization. This reflects moderate nonlinearity and the growing influence of fractional effects. At $\rho = 0.99$ (Figure 9(c)), the peak reaches its maximum sharpness and height, showing strong localization of energy–an essential trait in high-gain optical systems or pulse-shaping applications. The 2D plot provides a direct comparison of these profiles. It highlights how increasing ρ leads to sharper and taller soliton peaks, revealing how fractional-order dynamics enhance wave confinement and intensity. This makes such solutions highly relevant in the design of ultra-short optical pulses, where control over pulse sharpness and shape is critical for signal clarity and bandwidth efficiency. Figure 9 demonstrates how the conformable fractional derivative allows for tunable control over soliton characteristics. Bright solitons modeled here showcase how adjusting ρ can directly impact the wave intensity and spread, with practical applications in optical fiber communication, laser physics, and nonlinear wave engineering.

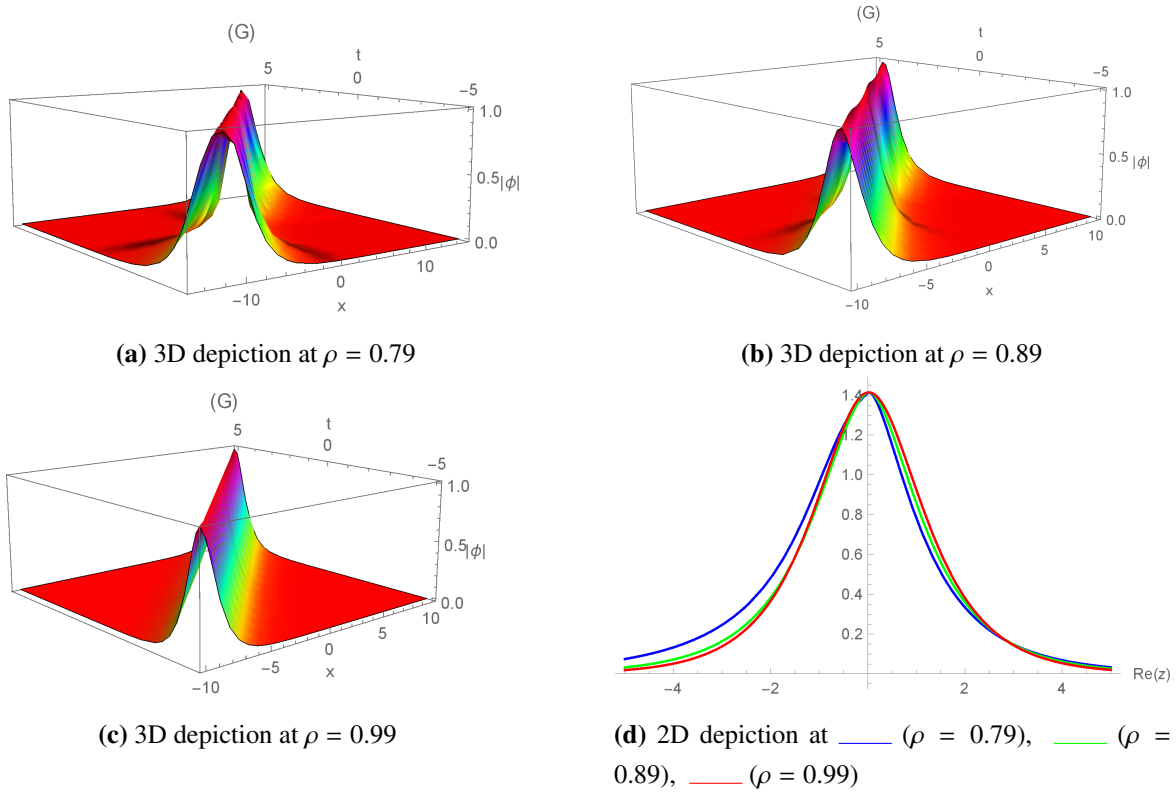

(a) 3D depiction at $\rho = 0.79$

(b) 3D depiction at $\rho = 0.89$

(c) 3D depiction at $\rho = 0.99$

(d) 2D depiction at ____ ($\rho = 0.79$), ____ ($\rho = 0.89$), ____ ($\rho = 0.99$)

Figure 9. The effect of fractional order in two- and three-dimensional models for a solution (4.90) with $\epsilon = 1$, $B = 2$, $\sigma = 1$, $\omega = 1$, $\nu = 1$, $\beta = 1$, $\delta = 2$, $k_2 = 2$, $k = 1.5$, $c_0 = 0$, $\gamma = 2$.

6. Conclusions

The fractional Akbota equation serves as an effective instrument for simulating soliton behavior in optical fiber telecommunications systems. By integrating memory effects and nonlocal interactions, it provides a more precise depiction of the nonlinear dynamics that regulate pulse propagation in fiber optics. The soliton solutions obtained from this equation may improve signal stability and transmission efficiency, tackling the issues of long-distance, high-data-rate communication. In order to accomplish this goal, we employ the mEDAM and new Kudryashov method. The models under consideration, being of the Heisenberg ferromagnetic kind, hold great importance in several nonlinear phenomena. The use of the conformable fractional derivative provides a tunable and physically meaningful enhancement to the classical model, allowing for better representation of complex wave dynamics in fiber-optic communication channels. Two- and three-dimensional graphs in Figures 1–9 illustrate periodic-singular, periodic, breather soliton, and bright soliton solutions of the obtained results. Graphs additionally display the fractional effect on solutions. These figures highlight how fractional parameters influence system behavior, making them useful for modeling adaptive signal processing and wave dynamics in engineering applications. The results gained have great utility in the fields of optics, telecommunications, fiber optics, and other fields. Therefore, the solutions obtained are useful for further research on these models. The various range of solutions is provided by the employed techniques. Our acquired solutions will be beneficial in the ongoing analysis of the relevant model.

This research gives a new contribution through the examination of the conformable fractional Akbota system by using up-to-date solution methods, achieving never-before-published bright, dark, periodic-singular, and breather solitons. The proposed methods and obtained findings assist in completing a lack of information and give a complete perspective on the dynamics of nonlinear waves with fractionals.

Author contributions

Patricia J.Y. Wong and Salah Mahmoud Boulaaras: Investigation, Formal analysis, Resources, Writing–review and editing; Musarat Bibi: Data curation, Formal analysis, Investigation, Resources, Validation, Writing–original draft; Muhammad S. Saleem: Conceptualization, Methodology, Software, Supervision, Visualization, Writing–original draft. All authors have read and agreed to the published version of the manuscript.

Use of Generative-AI tools declaration

The authors declare they have not used Artificial Intelligence (AI) tools in the creation of this article.

Acknowledgments

The authors gratefully acknowledge the School of Electrical and Electronic Engineering, Nanyang Technological University, Singapore, for their academic support and resources. Special thanks to the Department of Mathematics, University of Okara, Pakistan, and the Department of Mathematics, College of Science, Qassim University, Saudi Arabia, for laying the strong mathematical foundation essential to this work.

Conflict of interest

Dr. Patricia J.Y. Wong is a Guest Editor of the special issue "Inequalities & Partial Differential Equations" for AIMS Mathematics. Dr. Patricia J.Y. Wong was not involved in the editorial review and the decision to publish this article. The authors declare that they have no conflicts of interest.

References

1. E. M. E. Zayed, Y. A. Amer, R. M. A. Shohib, The fractional complex transformation for nonlinear fractional partial differential equations in the mathematical physics, *J. Assoc. Arab Univ. Basic Appl. Sci.*, **19** (2016), 59–69. https://doi.org/10.1016/j.jaubas.2014.06.008
2. H. G. Sun, Y. Zhang, D. Baleanu, W. Chen, Y. Q. Chen, A new collection of real world applications of fractional calculus in science and engineering, *Commun. Nonlinear Sci. Numer. Simul.*, **64** (2018), 213–231. https://doi.org/10.1016/j.cnsns.2018.04.019
3. J. Singh, D. Kumar, A. Kılıçman, Numerical solutions of nonlinear fractional partial differential equations arising in spatial diffusion of biological populations, *Abstr. Appl. Anal.*, **2014** (2014), 535793. https://doi.org/10.1155/2014/535793

4. A. Ara, N. A. Khan, O. A. Razzaq, T. Hameed, M. A. Z. Raja, Wavelets optimization method for evaluation of fractional partial differential equations: an application to financial modelling, *Adv. Differ. Equ.*, **2018** (2018), 1–13. https://doi.org/10.1186/s13662-017-1461-2
5. M. Şenol, Abundant solitary wave solutions to the new extended (3+1)-dimensional nonlinear evolution equation arising in fluid dynamics, *Mod. Phys. Lett. B*, **39** (2025), 2450475. https://doi.org/10.1142/S021798492450475X
6. L. Akinyemi, M. Şenol, U. Akpan, K. Oluwasegun, The optical soliton solutions of generalized coupled nonlinear Schrödinger-Korteweg-de Vries equations, *Opt. Quantum Electron.*, **53** (2021), 1–14. https://doi.org/10.1007/s11082-021-03030-7
7. M. Bilal, W. C. Hu, J. L. Ren, Different wave structures to the Chen-Lee-Liu equation of monomode fibers and its modulation instability analysis, *Eur. Phys. J. Plus*, **136** (2021), 385. https://doi.org/10.1140/epjp/s13360-021-01383-2
8. M. Bilal, J. L. Ren, Dynamics of exact solitary wave solutions to the conformable time-space fractional model with reliable analytical approaches, *Opt. Quantum Electron.*, **54** (2022), 40. https://doi.org/10.1007/s11082-021-03408-7
9. U. Younas, M. Bilal, J. L. Ren, Propagation of the pure-cubic optical solitons and stability analysis in the absence of chromatic dispersion, *Opt. Quantum Electron.*, **53** (2021), 1–25. https://doi.org/10.1007/s11082-021-03151-z
10. M. Bilal, J. L. Ren, M. Inc, R. T. Alqahtani, Dynamics of solitons and weakly ion-acoustic wave structures to the nonlinear dynamical model via analytical techniques, *Opt. Quantum Electron.*, **55** (2023), 656. https://doi.org/10.1007/s11082-023-04880-z
11. M. Bilal, H. Haris, A. Waheed, M. Faheem, The analysis of exact solitons solutions in monomode optical fibers to the generalized nonlinear Schrödinger system by the compatible techniques, *Int. J. Math. Comput. Eng.*, **1** (2023), 149–170. https://doi.org/10.2478/ijmce-2023-0012
12. A. Zafar, M. Ashraf, A. Saboor, A. Bekir, M-Fractional soliton solutions of fifth-order generalized nonlinear fractional differential equation via (G'/G^2)-expansion method, *Physica Scr.*, **99** (2024), 025242. https://doi.org/10.1088/1402-4896/ad1e45
13. S. Kaewta, S. Sirisubtawee, S. Koonprasert, S. Sungnul, Applications of the (G'/G^2)-expansion method for solving certain nonlinear conformable evolution equations, *Fractal Fract.*, **5** (2021), 88. https://doi.org/10.3390/fractalfract5030088
14. A. H. Ganie, M. M. AlBaidani, A. Khan, A comparative study of the fractional partial differential equations via novel transform, *Symmetry*, **15** (2023), 1101. https://doi.org/10.3390/sym15051101
15. J. L. Zhang, J. Q. Xie, W. Shi, Y. T. Huo, Z. K. Ren, D. P. He, Resonance and bifurcation of fractional quintic Mathieu-Duffing system, *Chaos*, **33** (2023), 023131. https://doi.org/10.1063/5.0138864
16. S. O. Abdulla, S. T. Abdulazeez, M. Modanli, Comparison of third-order fractional partial differential equation based on the fractional operators using the explicit finite difference method, *Alex. Eng. J.*, **70** (2023), 37–44. https://doi.org/10.1016/j.aej.2023.02.032
17. V. P. Dubey, D. Kumar, J. Singh, A. M. Alshehri, S. Dubey, Analysis of local fractional Klein-Gordon equations arising in relativistic fractal quantum mechanics, *Wav. Ran. Com. Media.*, **1** (2022), 113009. https://doi.org/10.1080/17455030.2022.2112993

18. V. R. Hosseini, W. Zou, The peridynamic differential operator for solving time-fractional partial differential equations, *Nonlinear Dyn.*, **109** (2022), 1823–1850. https://doi.org/10.1007/s11071-022-07424-4

19. S. Y. Lu, M. Z. Liu, L. R. Yin, Z. T. Yin, X. Liu, W. F. Zheng, The multi-modal fusion in visual question answering: a review of attention mechanisms, *PeerJ Comput. Sci.*, **9** (2023), e1400. https://doi.org/10.7717/peerj-cs.1400

20. S. Y. Lu, Y. M. Ding, M. Z. Liu, Z. T. Yin, L. R. Yin, W. F. Zheng, Multiscale feature extraction and fusion of image and text in VQA, *Int. J. Comput. Intell. Syst.*, **16** (2023), 54. https://doi.org/10.1007/s44196-023-00233-6

21. G. Nugmanova, Z. Zhunussova, K. Yesmakhanova, G. Mamyrbekova, R. Myrzakulov, Integrable Heisenberg Ferromagnet equations with self-consistent potentials, *Int. J. Phys. Math. Sci.*, **9** (2015), 472–475. https://doi.org/10.5281/zenodo.1107972

22. T. Mathanaranjan, R. Myrzakulov, Conservation laws, soliton solutions and stability analysis for the Akbota equation, 2023. https://doi.org/10.13140/RG.2.2.32430.08006

23. W. A. Faridi, M. A. Bakar, M. B. Riaz, Z. Myrzakulova, R. Myrzakulov, A. M. Mostafa, Exploring the optical soliton solutions of Heisenberg ferromagnet-type of Akbota equation arising in surface geometry by explicit approach, *Opt. Quantum Electron.*, **56** (2024), 1046. https://doi.org/10.1007/s11082-024-06904-8

24. Z. Li, S. Zhao, Bifurcation, chaotic behavior and solitary wave solutions for the Akbota equation, *AIMS Math.*, **9** (2024), 22590–22601. https://doi.org/10.3934/math.20241100

25. M. M. Tariq, M. B. Riaz, M. Aziz-ur-Rehman, Investigation of space-time dynamics of Akbota equation using Sardar sub-equation and Khater methods: unveiling bifurcation and chaotic structure, *Int. J. Theor. Phys.*, **63** (2024), 210. https://doi.org/10.1007/s10773-024-05733-5

26. T. Mathanaranjan, R. Myrzakulov, Integrable Akbota equation: conservation laws, optical soliton solutions and stability analysis, *Opt. Quantum Electron.*, **56** (2024), 564. https://doi.org/10.1007/s11082-023-06227-0

27. H. Y. Kong, R. Guo, Dynamic behaviors of novel nonlinear wave solutions for the Akbota equation, *Optik*, **282** (2023), 170863. https://doi.org/10.1016/j.ijleo.2023.170863

28. K. A. Gepreel, R. M. A. Shohib, M. E. M. Alngar, Analyzing multiplicative noise effects on stochastic resonant nonlinear Schrödinger equation via two integration algorithms, *Opt. Quantum Electron.*, **57** (2025), 156. https://doi.org/10.1007/s11082-025-08067-6

29. N. T. Trouba, H. Y. Xu, M. E. M. Alngar, R. M. A. Shohib, H. A. Mahmoud, X. Z. Zhu, Soliton solutions and stability analysis of the stochastic nonlinear reaction-diffusion equation with multiplicative white noise in soliton dynamics and optical physics, *AIMS Math.*, **10** (2025), 1859–1881. https://doi.org/10.3934/math.2025086

30. N. T. Trouba, M. E. M. Alngar, R. M. A. Shohib, H. A. Mahmoud, Y. Yildirim, H. Y. Xu, et al., Novel solitary wave solutions of the (3+1)-dimensional nonlinear Schrödinger equation with generalized Kudryashov self-phase modulation, *AIMS Math.*, **10** (2025), 4374–4411. https://doi.org/10.3934/math.2025202

31. R. Khalil, M. Al Horani, A. Yousef, M. Sababheh, A new definition of fractional derivative, *J. Comput. Appl. Math.*, **264** (2014), 65–70. https://doi.org/10.1016/j.cam.2014.01.002

32. A. Zafar, A. R. Seadawy, The conformable space-time fractional mKdV equations and their exact solutions, *J. King Saud Univ. Sci.*, **31** (2019), 1478–1484. https://doi.org/10.1016/j.jksus.2019.09.003

33. H. Yasmin, N. H. Aljahdaly, A. M. Saeed, R. Shah, Investigating symmetric soliton solutions for the fractional coupled Konno-Onno system using improved versions of a novel analytical technique, *Mathematics*, **11** (2023), 1–30. https://doi.org/10.3390/math11122686

34. H. Yasmin, N. H. Aljahdaly, A. M. Saeed, R. Shah, Probing families of optical soliton solutions in fractional perturbed Radhakrishnan-Kundu-Lakshmanan model with improved versions of extended direct algebraic method, *Fractal Fract.*, **7** (2023), 1–29. https://doi.org/10.3390/fractalfract7070512

35. M. Bilal, J. Iqbal, R. Ali, F. A. Awwad, E. A. A. Ismail, Exploring families of solitary wave solutions for the fractional coupled Higgs system using modified extended direct algebraic method, *Fractal Fract.*, **7** (2023), 1–33. https://doi.org/10.3390/fractalfract7090653

36. S. M. Mirhosseini-Alizamini, H. Rezazadeh, K. Srinivasa, A. Bekir, New closed form solutions of the new coupled Konno-Oono equation using the new extended direct algebraic method, *Pramana*, **94** (2020), 52. https://doi.org/10.1007/s12043-020-1921-1

37. H. Khan, S. Barak, P. Kumam, M. Arif, Analytical solutions of fractional Klein-Gordon and gas dynamics equations, via the $(G^{'}/G)$-expansion method, *Symmetry*, **11** (2019), 1–12. https://doi.org/10.3390/sym11040566

38. A. Biswas, A. Sonmezoglu, M. Ekici, M. Mirzazadeh, Q. Zhou, S. P. Moshokoa, et al., Optical soliton perturbation with fractional temporal evolution by generalized Kudryashov's method, *Optik*, **164** (2018), 303–310. https://doi.org/10.1016/j.ijleo.2018.03.032

39. R. Yadav, S. Malik, S. Kumar, R. Sharma, A. Biswas, Y. Yıldırım, et al., Highly dispersive W-shaped and other optical solitons with quadratic-cubic nonlinearity: symmetry analysis and new Kudryashov's method, *Chaos Solitons Fract.*, **173** (2023), 113675. https://doi.org/10.1016/j.chaos.2023.113675

40. D. Kumar, M. Kaplan, Application of the modified Kudryashov method to the generalized Schrödinger-Boussinesq equations, *Opt. Quantum Electron.*, **50** (2018), 1–14. https://doi.org/10.1007/s11082-018-1595-9

41. N. A. Kudryashov, Method for finding highly dispersive optical solitons of nonlinear differential equations, *Optik*, **206** (2020), 163550. https://doi.org/10.1016/j.ijleo.2019.163550